

# Gravitational Waves Induced by Scalar Perturbations with a Broken Power-law Peak

Chong-Zhi Li,<sup>1,2</sup> Chen Yuan,<sup>3,\*</sup> and Qing-Guo Huang<sup>1,2,4,†</sup>

<sup>1</sup>*CAS Key Laboratory of Theoretical Physics, Institute of Theoretical Physics,  
Chinese Academy of Sciences, Beijing 100190, China*

<sup>2</sup>*School of Physical Sciences, University of Chinese Academy of Sciences, No. 19A Yuquan Road, Beijing 100049, China*

<sup>3</sup>*CENTRA, Departamento de Física, Instituto Superior Técnico – IST,  
Universidade de Lisboa – UL, Avenida Rovisco Pais 1, 1049–001 Lisboa, Portugal*

<sup>4</sup>*School of Fundamental Physics and Mathematical Sciences Hangzhou  
Institute for Advanced Study, UCAS, Hangzhou 310024, China*

(Dated: July 19, 2024)

We propose an analytical approximation for the energy spectrum of the scalar induced gravitational waves (SIGWs) generated by a broken power-law power spectrum, and find that both the asymptotic power-law tails and the intermediate peak contribute distinct features to the SIGW spectrum. Moreover, the broken power-law power spectrum has abundant near-peak features and our results can be used as a near-peak approximation that covers a wide range of models. Our analytical approximation is useful in the rapid generation of the SIGW energy spectrum, which is beneficial for gravitational wave data analysis.

## I. INTRODUCTION

Gravitational waves (GWs) originating from cosmological processes offer an important approach to investigate the early universe, as they propagate almost freely in the cosmic background. Among various GWs, scalar-induced gravitational waves (SIGWs) are well-known as a secondary effect sourced by linear order scalar perturbations [1–7]. Additionally, SIGWs are closely connected with the formation of primordial black holes (PBHs) in the very early Universe [8–11].

According to the detection of the Cosmic Microwave Background (CMB) anisotropies [12, 13], the amplitude of the scalar power spectrum is constrained to be approximately  $A_s \approx 2.1 \times 10^{-9}$  across scales ranging from megaparsecs (Mpc) to gigaparsecs (Gpc), exhibiting a nearly scale-invariant feature, which is too small to generate detectable SIGWs. However, the information at scales smaller than Mpc lies beyond the reach of CMB detection, leaving open the possibility of significant amplitude of primordial scalar perturbations. In this context, SIGWs can provide constraints on primordial scalar power spectrum, inflationary models, and the expansion history of the universe [14–46].

Moreover, if a large scalar perturbation exceeds a critical value, the overdense region will collapse to form a PBH once the corresponding wavelength reenters the Hubble horizon. In this case, the abundance of PBHs is closely related to the amplitude of the scalar power spectrum, and hence will be tightly constrained by the observations on SIGWs, leading to the significance of studying both PBHs and SIGWs as complementary topics [46–66]. For reviews on SIGWs, see [67, 68].

Since the first detection of GW by LIGO, numerous GW events have been detected by the LIGO-Virgo-KAGRA collaborations [69–74]. It is possible that some of the events have primordial origins, implying that the corresponding primordial perturbations would generate SIGWs in the frequency band of Pulsar Timing Arrays (PTAs). Recently, hints of the stochastic GW background have been reported by the PTA collaborations [75–83]. Alongside various astrophysical and cosmological explanations (see, for example, [84, 85]), a potential interpretation is that this signal originates from SIGWs [86–95]. Furthermore, SIGWs are expected to be detected by future space-based GW detectors such as LISA [96], Taiji [97], TianQin [98] and DECIGO [99]. These observations will place constraints on the abundance of PBH potentially addressing the remaining mass window where PBHs could constitute a significant fraction of dark matter [100–102].

Based on the semi-analytical formula derived [32–34], the SIGW energy spectrum has been studied for specific cases and some results will be relevant to this work. During the radiation-dominated (RD) era, the infrared (IR) behavior is derived in [37], assuming a general enhanced scalar power spectrum with both IR and ultraviolet (UV) cutoffs. In this case, the GW spectrum scales as  $k^3 \ln^2 k$  if  $k$  is much smaller than the width of remaining interval, while it shows a transition to  $k^2 \ln^2 k$  if the width is extremely small. As a special case, SIGWs arise from a log-normal scalar power

\* Corresponding author: [chenyuan@tecnico.ulisboa.pt](mailto:chenyuan@tecnico.ulisboa.pt)

† Corresponding author: [huangqg@itp.ac.cn](mailto:huangqg@itp.ac.cn)

spectrum were studied in [103] for the widths  $\Delta \ll 1$  and  $\Delta \gtrsim 1$  respectively. In this paper, we analytically calculate the SIGW spectrum with the scalar power spectrum possessing a broken power-law feature with a smooth transition, which can typically be generated by single-field inflation models [40, 45, 104, 105]. This power spectrum also contains abundant features such as near-peak asymmetry and asymptotic power-law tails, which would lead to characteristic structures in the SIGW spectrum.

This paper is organized as follows. We briefly review the formula of GW spectrum during RD era in Sec. II, and consider the broken power-law power spectrum in Sec. III. We present the approximation on the power spectrum first in Sec. III A and the GW spectrum is calculated in Sec. III B, where the asymptotic behavior and the comparison to the numerical result is also presented. Finally, we summarize our findings in Sec. IV. To streamline the calculations, a quick approach can be taken by starting from the final result, Eq. (55), and referring back to the intermediate results as needed.

## II. SIGW DURING RD ERA

In this section, we will briefly review the SIGWs generated during the RD era. Considering scalar and tensor perturbations only, the perturbed Friedmann-Robertson-Walker (FRW) metric in Newtonian gauge can be written as

$$ds^2 = a^2(\eta) \left[ -(1 + 2\phi)d\eta^2 + \left( (1 - 2\phi)\delta_{ij} + \frac{h_{ij}}{2} \right) dx^i dx^j \right], \quad (1)$$

where  $\phi$  is the linear scalar perturbation and  $h_{ij}$  refers to the second-order tensor perturbation. For SIGWs in different gauges, see [106–111]. During the RD era, the equations of motion for  $\phi$  and  $h_{ij}$  in Fourier space can be written as

$$\phi''_{\mathbf{k}}(\eta) + 4\mathcal{H}\phi'_{\mathbf{k}}(\eta) + \frac{1}{3}k^2\phi_{\mathbf{k}}(\eta) = 0, \quad (2)$$

$$h''_{\mathbf{k},\lambda}(\eta) + 2\mathcal{H}h'_{\mathbf{k},\lambda}(\eta) + k^2h_{\mathbf{k},\lambda}(\eta) = \mathcal{S}_\lambda(\mathbf{k}, \eta). \quad (3)$$

The prime denotes the derivative with respect to the conformal time  $\eta$ ,  $\lambda$  denotes the two polarization modes orthogonal to  $\mathbf{k}$ , and  $\mathcal{S}_\lambda$  is the source term up to  $\phi_{\mathbf{k}}^2$  order. Here  $\phi_{\mathbf{k}}(\eta)$  and  $\mathcal{S}_\lambda(\mathbf{k}, \eta)$  take the form:

$$\phi(\mathbf{k}, \eta) \equiv \phi_{\mathbf{k}}T_\phi(k\eta) = \phi_{\mathbf{k}} \frac{9}{(k\eta)^2} \left( \frac{\sin(k\eta/\sqrt{3})}{k\eta/\sqrt{3}} - \cos(k\eta/\sqrt{3}) \right), \quad (4)$$

$$\mathcal{S}_\lambda(\mathbf{k}, \eta) = -4 \int \frac{d^3p}{(2\pi)^{3/2}} (e_\lambda^{ij} p_i p_j) \phi_{\mathbf{p}} \phi_{\mathbf{k}-\mathbf{p}} F(p/k, |\mathbf{k}-\mathbf{p}|/k, k\eta), \quad (5)$$

$$F(u, v, x) = 3T_\phi(ux)T_\phi(vx) + uxT'_\phi(ux)T_\phi(vx) + vxT_\phi(ux)T'_\phi(vx) + uvx^2T'_\phi(ux)T'_\phi(vx), \quad (6)$$

where  $\phi_{\mathbf{k}}$  is the initial condition given by inflation models and  $e_\lambda^{ij}$  is the polarization tensor corresponding to  $\lambda$ . The solution of Eq. (3) can thus be obtained using the Green's function method:

$$h_\lambda(\mathbf{k}, \eta) = \int_0^\eta d\eta' \frac{\sin(k(\eta - \eta'))}{k} \frac{a(\eta')}{a(\eta)} \mathcal{S}_\lambda(\mathbf{k}, \eta'). \quad (7)$$

An observational quantity that characterize the SIGW is the energy spectrum, which is defined as GW energy density per logarithm wavelength and normalized by the critical energy  $\rho_c$ :

$$\Omega_{\text{GW}}(\mathbf{k}, \eta) = \frac{1}{\rho_c} \frac{d\rho_{\text{GW}}}{d \ln k} \approx \frac{k^5}{96\pi^2 \mathcal{H}^2} \sum_\lambda \overline{\langle h_\lambda(\mathbf{k}, \eta) h_\lambda(-\mathbf{k}, \eta) \rangle}. \quad (8)$$

The overline in Eq. (8) stands for oscillating average on  $\eta$ . The energy spectrum of SIGW can be reduced to that of primordial power spectrum of  $\phi$  such that:

$$\Omega_{\text{GW}}(\mathbf{k}, \eta) = \frac{1}{6} \int_0^{+\infty} dv \int_{|1-v|}^{1+v} du \frac{v^2}{u^2} \left[ 1 - \left( \frac{1+v^2-u^2}{2v} \right)^2 \right]^2 \mathcal{P}_\phi(uk) \mathcal{P}_\phi(vk) \overline{I^2(u, v, k\eta)}, \quad (9)$$

$$I(u, v, x) \equiv \frac{1}{2} \int_0^x d\tilde{x} \tilde{x} \sin(x - \tilde{x}) (F(u, v, \tilde{x}) + F(v, u, \tilde{x})). \quad (10)$$

The transformation has been performed in the integral that  $u = p/k$ ,  $v = |\mathbf{p} - \mathbf{k}|/k$ . Here the dimensionless power spectrum of scalar perturbation  $\mathcal{P}_\phi(\mathbf{k})$  is defined as:

$$\langle \phi_{\mathbf{k}} \phi_{\mathbf{k}'} \rangle \equiv \frac{2\pi^2}{k^3} \mathcal{P}_\phi(\mathbf{k}) \delta(\mathbf{k} + \mathbf{k}'). \quad (11)$$

Furthermore, we have neglected the connected four-point correlation function, which vanishes if the distribution of  $\phi$  is Gaussian. For contributions from the non-Gaussianities, see e.g. [42, 112, 113]. The integral  $\overline{I^2(u, v, k\eta)}$  in Eq. (10) was calculated in [32, 33] with the limit  $k\eta \rightarrow +\infty$  in which the scalar perturbations have almost decayed to zero. Consequently,  $\Omega_{\text{GW}}$  in the RD era can be written as

$$\Omega_{\text{GW}}(k) = \int_0^{+\infty} dv \int_{|1-v|}^{1+v} du \mathcal{T}(u, v) \mathcal{P}_{\mathcal{R}}(uk) \mathcal{P}_{\mathcal{R}}(vk), \quad (12)$$

$$\mathcal{T}(u, v) = \frac{3}{1024u^8v^8} (u^2 + v^2 - 3)^4 (1 - (u - v)^2)^2 (1 - (u + v)^2)^2 \left( \pi^2 \Theta(u + v - \sqrt{3}) + \left( \ln \frac{3 - (u - v)^2}{|3 - (u + v)^2|} + \frac{4uv}{u^2 + v^2 - 3} \right)^2 \right). \quad (13)$$

We have converted the scalar perturbation to the comoving curvature perturbation  $\mathcal{R} = (3/2)\phi$ . In this study, we neglect the QCD effects where the equation of state and the sound speed slightly decrease from 1/3 during the RD era, as discussed in [114].

In the following section, we will show a detailed calculation on Eq. (12) in the circumstance that  $\mathcal{P}_{\mathcal{R}}$  has a broken power-law feature, which inspires further discussion.

### III. BROKEN POWER-LAW FEATURE

In this section, the curvature perturbation with a broken power-law feature in the power spectrum will be considered:

$$\mathcal{P}_{\text{PL}}(k) = A \frac{\alpha + \beta}{\beta(k/k_*)^{-\alpha} + \alpha(k/k_*)^\beta}. \quad (14)$$

The spectrum has a single peak at  $k = k_*$  and is normalized by  $\mathcal{P}_{\text{PL}}(k_*) = A$ . After leaving the peak,  $\mathcal{P}_{\text{PL}}(k)$  decays as a power-law with the power exponent  $\alpha$  and  $-\beta$  respectively in the  $k \rightarrow 0$  and  $k \rightarrow +\infty$  regions. Further discussion on the features of power spectrum will be presented in Sec. III A, which will be used in the analytical approach to  $\Omega_{\text{GW}}$  in Sec. III B.

The broken power-law peak is typically derived from single-field inflation and the parameter is further restricted by  $\alpha < 4$  [40, 45, 104, 105]. Additionally, the coefficient of near-peak expansion is independent up to the  $(k - k_*)^3$  order, which means that the broken power-law peak is always a reasonable near-peak approximation even if it is highly asymmetric on both sides. Therefore, we neglect the restriction on the parameter to step further to a general situation.

In the following sections, we use the dimensionless variable  $\kappa = k/k_*$  instead, and refer to  $\mathcal{P}_{\mathcal{R}}(\kappa)$  as  $\mathcal{P}_{\text{PL}}(k)$  for simplicity if no ambiguity would happen.

#### A. Features and extreme cases

In this part, we reduce the power spectrum to a simpler form and enumerate the detailed features of a broken power-law peak, extending the approach to more general cases.

The most distinctive feature of a broken power-law spectrum is the power-law expansion on  $\kappa = 0$  and  $\kappa \rightarrow +\infty$ :

$$\mathcal{P}_{\mathcal{R}}(\kappa) = A \begin{cases} (1 + \lambda)\kappa^\alpha \sum_{n=0}^{\infty} (-1)^n K^n(\kappa) & \text{for } K(\kappa) < 1, \\ (1 + \lambda^{-1})\kappa^{-\beta} \sum_{n=0}^{\infty} (-1)^n K^{-n}(\kappa) & \text{for } K(\kappa) > 1, \end{cases} \quad (15)$$

$$\delta_{IR} = (-1)^n K^{1+n}(\kappa), \quad \delta_{UV} = (-1)^n K^{-1-n}(\kappa). \quad (16)$$

$\lambda = \alpha/\beta$  and  $K(\kappa) = \lambda\kappa^{\alpha+\beta}$  are introduced for simplicity, and  $\delta$  is the relative error of the power expansion to  $K^n$  term. To the leading order, the series is reduced to  $n = 0$  term. We assume that the power-law feature is broken

when the leading order of the asymptotic expansion reaches the peak value, where  $\kappa$  and  $\mathcal{P}_{\mathcal{R}}(\kappa)$  satisfy:

$$\begin{aligned} \kappa_- &= (1 + \lambda)^{-1/\alpha}, \quad \kappa_0 = \lambda^{-1/(\alpha+\beta)}, \quad \kappa_+ = (1 + \lambda^{-1})^{1/\beta}, \quad \kappa_- < \kappa_0 < \kappa_+, \\ \mathcal{P}_{\mathcal{R}}(\kappa_-) &> \frac{A}{2}, \quad \mathcal{P}_{\mathcal{R}}(\kappa_+) > \frac{A}{2}, \quad \mathcal{P}_{\mathcal{R}}(\kappa_+)\mathcal{P}_{\mathcal{R}}(\kappa_-) > \frac{A^2}{2}, \end{aligned}$$

where  $\kappa_-$  and  $\kappa_+$  are the critical values of IR and UV expansion respectively, and  $\kappa_0$  is the boundary of the convergence domain of Eq. (15). The relation indicates that even if we connect the leading order tail with the transition part replaced by the peak value, the relative error is smaller than 1, and approaches 1 only if the power index is much larger than that on the other side, i.e.,  $|\ln(\alpha/\beta)| \gg 1$ . In order to elevate the approximation to a higher accuracy, we introduce a variable transformation that maintains  $\mathcal{P}_{\mathcal{R}}$ :

$$\mathcal{P}_{\mathcal{R}}(\alpha, \beta; \kappa) = \mathcal{P}_{\mathcal{R}}(\lambda, 1, \kappa^\beta) = \mathcal{P}_{\mathcal{R}}(\lambda^{-1}, 1, \kappa^{-\alpha}), \quad (17)$$

Therefore, once the approximation of  $\mathcal{P}_{\mathcal{R}}(\lambda, 1, \kappa^\beta)$  on  $0 < \kappa < 1$  and  $\lambda > 0$  is finished, it can be extended to the complete parameter space  $\alpha, \beta, \kappa > 0$  with the accuracy preserved. The the selection is based on that  $\kappa_-^\beta = (1 + \lambda)^{-1/\lambda} > e^{-1}$ , which make it convenient to extend the power-law tail to the peak with a quadratic polynomial. On the region  $\kappa < \kappa_-$ , the deviation of the power-law tail from  $\mathcal{P}_{\mathcal{R}}$  is roughly to the order  $(2\lambda + 1)$ , and consequently a general  $\mathcal{P}_{\mathcal{R}}(\kappa)$  can be approximated by:

$$\mathcal{P}_{\mathcal{R}}(\lambda, 1, \kappa) \approx A \begin{cases} (1 + \lambda)\kappa^\lambda + (\mathcal{P}_{\mathcal{R}}(\kappa_-) - 1)(\kappa/\kappa_-)^{(2\lambda+1)}, & \text{for } \kappa < \kappa_-; \\ 1 + (\mathcal{P}_{\mathcal{R}}(\kappa_-) - 1)[(\kappa - 1)/(\kappa_- - 1)]^2, & \text{for } \kappa_- < \kappa < 1. \end{cases} \quad (18)$$

$$\mathcal{P}_{\mathcal{R}}(\alpha, \beta, \kappa) = A \begin{cases} \mathcal{P}_{\mathcal{R}}(\lambda, 1, \kappa^\beta), & \text{for } \kappa < 1; \\ \mathcal{P}_{\mathcal{R}}(\lambda^{-1}, 1, \kappa^{-\alpha}), & \text{for } \kappa > 1. \end{cases} \quad (19)$$

Additionally,  $\mathcal{P}_{\mathcal{R}}^2(\kappa)$  will be used in the calculation of  $\Omega_{\text{GW}}$ , since it is associated with the  $p = |\mathbf{k} - \mathbf{p}|$  slice in Eq. (5), which separates the integral into two identical parts:

$$\mathcal{P}_{\mathcal{R}}^2(\alpha, \beta, \kappa) \approx A^2 \begin{cases} (1 + \lambda)^2 \kappa^{2\alpha} (1 + d_1 \kappa^{\beta+\alpha})^2, & \text{for } \kappa < \kappa_-; \\ 1 + d_2 (\kappa^\beta - 1)^2, & \text{for } \kappa_- < \kappa < 1; \\ 1 + d_3 (\kappa^{-\alpha} - 1)^2, & \text{for } 1 < \kappa < \kappa_+; \\ (1 + \lambda^{-1})^2 \kappa^{-2\beta} (1 + d_4 \kappa^{-\alpha-\beta})^2, & \text{for } \kappa > \kappa_+. \end{cases} \quad (20)$$

$$d_1 = \frac{\mathcal{P}_{\mathcal{R}}(\kappa_-) - 1}{\kappa_-^{\alpha+\beta}(1 + \lambda)}, \quad d_2 = \frac{\mathcal{P}_{\mathcal{R}}^2(\kappa_-) - 1}{(\kappa_-^\beta - 1)^2}, \quad d_3 = \frac{\mathcal{P}_{\mathcal{R}}^2(\kappa_+) - 1}{(\kappa_+^{-\alpha} - 1)^2}, \quad d_4 = \frac{\mathcal{P}_{\mathcal{R}}(\kappa_+) - 1}{(1 + \lambda^{-1})} \kappa_+^{\alpha+\beta}. \quad (21)$$

We have used that  $\kappa_-(\lambda, 1) = \kappa_-^\beta(\alpha, \beta)$ .

Moreover, as have been mentioned, a peaked spectrum can always be regarded as broken power-law near the peak, and therefore Eqs. (18)-(21) can be directly used for a near-peak approximation. The correspondence can be realized by match the power expansion at  $\kappa = 1$ , and we enumerate several representative peak for example:

$$\mathcal{P}_{\text{LN}}(k) = A \exp\left\{-\frac{\ln^2(k/k_*)}{2\Delta^2}\right\} \approx \mathcal{P}_{\text{PL}}(\Delta^{-1}, \Delta^{-1}, k), \quad (22)$$

$$\mathcal{P}_{\text{CLN}}(k) = A \exp\left\{-\lambda_1 \left(\frac{k}{k_*} - 1 - \ln \frac{k}{k_*}\right) - \lambda_2 \ln^2 \frac{k}{k_*}\right\} \approx \mathcal{P}_{\text{PL}}\left(\frac{c_2 - c_1}{2}, \frac{c_2 + c_1}{2}, k\right), \quad (23)$$

where  $c_1 = \lambda_1/(\lambda_1 + 2\lambda_2)$ ,  $c_2 = (8\lambda_2 + 4\lambda_1 + 4c_1^2)^{1/2}$ , and furthermore, some specific limit gives more trivial spectrum:

$$\lim_{\alpha, \beta \rightarrow 0} \mathcal{P}_{\mathcal{R}}(\alpha, \beta, \kappa) = A, \quad (24)$$

$$\lim_{\alpha \rightarrow \infty} \mathcal{P}_{\mathcal{R}}\left(\alpha, \frac{\alpha}{\kappa_-^\alpha - 1}, \kappa\right) = A \Theta(\kappa - \kappa_-), \quad (25)$$

$$\lim_{\alpha, \beta \rightarrow \infty} \frac{\sqrt{\alpha\beta}}{\pi} \frac{\lambda^{\frac{1}{2} \frac{\lambda-1}{\lambda+1}}}{\csc(\pi/(\lambda+1))} \mathcal{P}_{\mathcal{R}}(\alpha, \beta, \kappa) = A \delta(\kappa - 1). \quad (26)$$

It can be verified that the approximation in Eqs. (18)-(21) maintain the limit, but it should be noticed that the confusion between the near-peak approximation and the limit to delta function will lead to a deviation considering the different decay modes.

## B. Analytical approach to SIGW

In this part, we will calculate the GW spectrum derived in Sec. II, with the scalar spectrum  $\mathcal{P}_{\mathcal{R}}$  having a broken power-law feature as Eq. (14). To make use of the symmetry, we perform the transformation  $x = \frac{1}{\sqrt{2}}(u+v)$ ,  $y = \frac{1}{\sqrt{2}}(u-v)$  on the integral in Eq. (12):

$$\Omega_{\text{GW}}(k) = \int_{-\frac{1}{\sqrt{2}}}^{+\infty} dx \int_{-\frac{1}{\sqrt{2}}}^{\frac{1}{\sqrt{2}}} dy (1-2y^2)^2 F(x, y) \mathcal{P}_{\mathcal{R}} \left[ q \left( 1 + \frac{y}{x} \right) \right] \mathcal{P}_{\mathcal{R}} \left[ q \left( 1 - \frac{y}{x} \right) \right], \quad (27)$$

$$F(x, y) = \frac{3(1-2x^2)^2(x^2+y^2-3)^4}{4(x^2-y^2)^8} \left[ \pi^2 \Theta \left( x - \frac{\sqrt{6}}{2} \right) + \left( \ln \frac{3-2y^2}{|3-2x^2|} + \frac{2(x^2-y^2)}{x^2+y^2-3} \right)^2 \right], \quad (28)$$

where we have defined  $q = \kappa x / \sqrt{2}$  for simplicity. Obviously, most of the factors of  $F(x, y)$  are not sensitive to  $y$  since  $y^2 < 1/2$ , except for the region near the zero point of  $(x^2 + y^2 - 3)$  and  $(x^2 - y^2)$ . The former contributes little deviation to  $\Omega_{\text{GW}}$  since it is suppressed by the integration on the nearby peak if  $\mathcal{P}_{\mathcal{R}}$  has a width  $\gtrsim 10^{-1}$ , while below that the leading order of  $y$  is much smaller than that of  $x$ . Therefore, we consider the region  $x > \sqrt{6}/2$  first and regard  $y$  as a perturbation in  $F(x, y)$ :

$$\Omega_{\text{GW}}^{x > \frac{\sqrt{6}}{2}}(k) = \frac{3}{4} \int_{\frac{\sqrt{6}}{2}}^{+\infty} dx x^{-16} (1-2x^2)^2 (x^2-3)^4 \left[ \pi^2 + \left( \frac{2x^2}{x^2-3} - \ln \left( \frac{2}{3}x^2 - 1 \right) \right)^2 \right] \mathcal{P}_{\mathcal{R}}^2(q) Q(x, q), \quad (29)$$

$$\begin{aligned} Q(x, q) &\approx \int_{-\frac{1}{\sqrt{2}}}^{\frac{1}{\sqrt{2}}} dy (1-2y^2)^2 \left( 1 + F^{-1}(x, 0) \frac{1}{2} \frac{\partial^2 F(x, y)}{\partial y^2} y^2 \right) \mathcal{P}_{\mathcal{R}} \left[ q \left( 1 + \frac{y}{x} \right) \right] \mathcal{P}_{\mathcal{R}} \left[ q \left( 1 - \frac{y}{x} \right) \right] \mathcal{P}_{\mathcal{R}}^{-2}(q), \\ &\approx \int_{-\frac{1}{\sqrt{2}}}^{\frac{1}{\sqrt{2}}} dy (1-2y^2)^2 \left( 1 + 4 \frac{y^2}{x^2} \right) \mathcal{P}_{\mathcal{R}} \left[ q \left( 1 + \frac{y}{x} \right) \right] \mathcal{P}_{\mathcal{R}} \left[ q \left( 1 - \frac{y}{x} \right) \right] \mathcal{P}_{\mathcal{R}}^{-2}(q). \end{aligned} \quad (30)$$

$Q(x, q)$  refers to the contribution from the integration on  $y$  relative to the  $x = 0$  slice. In the last step, the approximation is performed in the sense of integration, so that the singularity of  $y^2$  order near  $x = \sqrt{3}$  has been neglected, while it is guaranteed at  $x = \sqrt{6}/2$  and  $x \rightarrow +\infty$ . The  $x^{-2}$  dependence is selected for further convenience.

Similarly, we can expand the  $\mathcal{P}_{\mathcal{R}}$  factors in Eq. (30) up to  $y^2/x^2$  order but a positive integrand should be guaranteed. Therefore, we replace the  $x$ -dependent factors in Eq. (30) with an exponential factor and mark the integral as  $\bar{Q}(x, q)$ :

$$\bar{Q}(x, q) = \int_{-\frac{1}{\sqrt{2}}}^{\frac{1}{\sqrt{2}}} dy (1-2y^2)^2 \exp \left\{ \frac{4-\gamma(q)}{x^2} y^2 \right\} = \frac{\sqrt{\pi} (c^2 + 2c + 3) \operatorname{erfi} \left( \frac{\sqrt{c/2}}{c} \right)}{c^{5/2}} - \frac{\sqrt{2}(c+3)e^{c/2}}{c^2}, \quad (31)$$

$$c(x, q) = \frac{4-\gamma(q)}{x^2}, \quad \gamma(q) = \alpha\beta \frac{\beta + (\alpha^2 + 2\alpha\beta + \alpha + (\beta-1)\beta) q^{\alpha+\beta} - \alpha q^{2(\alpha+\beta)}}{(\beta + \alpha q^{\alpha+\beta})^2}, \quad (32)$$

where  $\operatorname{erfi}(z) = -i \operatorname{erf}(iz)$  denotes the imaginary error function.  $\gamma(q)$  denotes a constant-order transition with the asymptotic behavior that  $\gamma(0) = \alpha$ ,  $\gamma(1) = \alpha\beta$  and  $\gamma(+\infty) = -\beta$ , which are related to the IR tail, peak and the UV tail of the power spectrum respectively. Looking back to Eq. (29), it remains difficult if we use Eq. (31) directly, but it becomes simpler if we focus on the specific values of  $\gamma(q)$  mentioned above. Also, it is helpful to take into account the approximation derived in Eq. (20) here, which also provides a segmentation to perform further approximation on  $\bar{Q}(x, q)$ .

In the case of  $\alpha\beta \leq 6$ , which means that the width of the peak on  $y$  direction  $(\alpha\beta\kappa^2)^{-1/2}$  have not entered that of  $(1-2y^2)^2$  before the peak leaving this region, we take the expansion of Eq. (31) at  $c = 0$  to the first order:

$$\bar{Q}(x, q) \approx \frac{8\sqrt{2}}{15} \left( 1 + \frac{1}{14} \frac{4-\gamma(q)}{x^2} \right). \quad (33)$$

We simply let  $\gamma(q) = \alpha\beta$  for  $\kappa_- < q < \kappa_+$  as a near-peak case. Considering that the IR and UV part of  $\mathcal{P}_{\mathcal{R}}$  may also take over the leading order of  $\Omega_{\text{GW}}(k)$ , we connect the asymptotic behavior of  $\gamma(q)$  and then  $\bar{Q}(x, q)$  can be

approximated for  $\alpha\beta \leq 6$ :

$$Q_c(x, \kappa) = \begin{cases} a_0 + a_{-2}x^{-2} & \text{for } x < \sqrt{2}\kappa_-/\kappa, \\ b_0 + b_{-2}x^{-2} & \text{for } \sqrt{2}\kappa_-/\kappa \leq x \leq \sqrt{2}\kappa_+/\kappa, \\ c_0 + c_{-2}x^{-2} + c_{-4}x^{-4} & \text{for } x > \sqrt{2}\kappa_+/\kappa, \end{cases} \quad (34)$$

$$a_{-2} = \frac{Q_c(\sqrt{2}\kappa_-/\kappa, \kappa) - \bar{Q}(\sqrt{6}/2, \sqrt{3}\kappa/2)}{(\sqrt{2}\kappa_-/\kappa)^{-2} - 2/3}, \quad a_0 = Q_c(\sqrt{2}\kappa_-/\kappa, \kappa) - (\sqrt{2}\kappa_-/\kappa)^{-2}a_{-2},$$

$$b_0 = c_0 = \frac{8\sqrt{2}}{15}, \quad b_{-2} = \frac{b_0}{14}(4 - \alpha\beta), \quad c_{-2} = \frac{c_0}{14}(4 + \beta), \quad c_{-4} = -\frac{c_0}{14}\beta(1 + \alpha) \left( \frac{\sqrt{2}\kappa_+}{\kappa} \right)^2.$$

Here we use  $\kappa$  as a variable instead of  $q$ . The higher order  $x^{-4}$  is introduced to guarantee the continuity of  $Q_c(x, \kappa)$  at  $x = \sqrt{2}\kappa_+/\kappa$ , which will further guarantee the continuity of the derivative of  $\Omega_{\text{GW}}(k)$ . As for the  $x < \sqrt{2}\kappa_-/\kappa$  region, it is the first priority to ensure the accuracy at  $x = \sqrt{6}/2$ , and the asymptotic behavior on  $\kappa \rightarrow 0$  turn into Eq. (33) naturally with  $\gamma(q) = \alpha$ .

For the other case  $\alpha\beta > 6$  where the approximation on  $c(x, q) \ll 1$  breaks down, we focus on the value of  $\bar{Q}(x, q)$  at  $q = 1$  first:

$$\bar{Q}(x, 1) \approx \left( \left( \frac{\sqrt{\pi}x}{\sqrt{\alpha\beta - 4}} \right)^{-2} + \left( \frac{8\sqrt{2}}{15} \right)^{-2} \right)^{-1/2}. \quad (35)$$

We have connected the leading order of  $x \ll \sqrt{\alpha\beta - 4}$  and  $x \gg \sqrt{\alpha\beta - 4}$ , with the relative error  $< 0.05$  compared with Eq. (31). We use the expansion of Eq. (35) at  $x = \sqrt{2}/\kappa$  as a near-peak approximation for  $\kappa_- < q < \kappa_+$ :

$$Q_c(x, \kappa) = \left( \frac{1}{\kappa} \sqrt{\frac{2\pi}{(\alpha\beta - 4)(\Delta_\kappa + 1)}} \right) \frac{\Delta_\kappa + \kappa x/\sqrt{2}}{\Delta_\kappa + 1}, \quad \Delta_\kappa = \frac{225}{128} \frac{2\pi}{\kappa^2(\alpha\beta - 4)}. \quad (36)$$

The feature of Eq. (36) depend on the value of  $\Delta_\kappa$ . The value of the second factor of  $Q_c(x, \kappa)$  falls between  $\kappa_-$  and  $\kappa_+$  and simply reduces to 1 when  $x = \sqrt{2}/\kappa$  or  $\Delta_\kappa \gg 1$ , while the overall coefficient gives a transition from  $\kappa^{-1}$  to constant near  $\Delta_\kappa = 1$ , and the constant limit returns to that in Eq. (33). Similarly, we connect the asymptotic behavior to the near-peak approximation and the result for  $\alpha\beta > 6$  can be written as:

$$Q_c(x, \kappa) = \begin{cases} a_0 + a_{-2}x^{-2} & \text{for } x < \sqrt{2}\kappa_-/\kappa, \\ b_0 + b_1x & \text{for } \sqrt{2}\kappa_-/\kappa \leq x \leq \sqrt{2}\kappa_+/\kappa, \\ c_0 + c_{-2}x^{-2} + c_{-4}x^{-4} & \text{for } x > \sqrt{2}\kappa_+/\kappa, \end{cases} \quad (37)$$

$$c_{-4} = \left( Q_c(\sqrt{2}\kappa_+/\kappa, \kappa) - c_0 - c_{-2} \left( \frac{\sqrt{2}\kappa_+}{\kappa} \right)^{-2} \right) \left( \frac{\sqrt{2}\kappa_+}{\kappa} \right)^4.$$

$a_0, a_{-2}, c_0$  and  $c_{-2}$  have the same form with that in Eq. (34), while  $b_0$  and  $b_1$  can be obtained from Eq. (36).

For both  $\alpha\beta \leq 6$  and  $\alpha\beta > 6$ ,  $Q(x, q)$  has been reduced to the sum of a group of  $x^{\rho_i}$  terms and the coefficients have been expressed as  $a_{\rho_i}, b_{\rho_i}$  and  $c_{\rho_i}$  which is related to IR, near-peak and UV region of the power spectrum respectively. The contribution to  $\Omega_{\text{GW}}$  can be written down directly by combining Eqs. (20) (29) (34) and (37), while

the parameters are also relevant to Eq. (31):

$$\Omega_{\text{GW}}^{x > \frac{\sqrt{6}}{2}}(k) = \Omega_{\text{GW}}^{q < \kappa_-}(k) + \Omega_{\text{GW}}^{\kappa_- < q < 1}(k) + \Omega_{\text{GW}}^{1 < q < \kappa_+}(k) + \Omega_{\text{GW}}^{q > \kappa_+}(k), \quad (38a)$$

$$\Omega_{\text{GW}}^{q < \kappa_-}(k) \approx A^2 (1 + \lambda)^2 \sum_{\rho_i} \sum_{j=0}^2 a_{\rho_i} C_2^j d_1^j \left( \frac{\kappa}{\sqrt{2}} \right)^{2\alpha + j(\alpha + \beta)} \Omega(\rho_i + 2\alpha + j(\alpha + \beta), x) \Big|_{\frac{\sqrt{6}}{2}}^{R_1}, \quad (38b)$$

$$\Omega_{\text{GW}}^{\kappa_- < q < 1}(k) \approx A^2 \sum_{\rho_i} b_{\rho_i} \left( \Omega(\rho_i, x) + d_2 \sum_{j=0}^2 C_2^j (-1)^j \left( \frac{\kappa}{\sqrt{2}} \right)^{j\beta} \Omega(\rho_i + j\beta, x) \right) \Big|_{R_1}^{R_2}, \quad (38c)$$

$$\Omega_{\text{GW}}^{1 < q < \kappa_+}(k) \approx A^2 \sum_{\rho_i} b_{\rho_i} \left( \Omega(\rho_i, x) + d_3 \sum_{j=0}^2 C_2^j (-1)^j \left( \frac{\kappa}{\sqrt{2}} \right)^{-j\alpha} \Omega(\rho_i - j\alpha, x) \right) \Big|_{R_2}^{R_3}, \quad (38d)$$

$$\Omega_{\text{GW}}^{q > \kappa_+}(k) \approx A^2 (1 + \lambda^{-1})^2 \sum_{\rho_i} \sum_{j=0}^2 c_{\rho_i} C_2^j d_4^j \left( \frac{\kappa}{\sqrt{2}} \right)^{-2\beta - j(\alpha + \beta)} \Omega(\rho_i - 2\beta - j(\alpha + \beta), x) \Big|_{R_3}^{+\infty}. \quad (38e)$$

Here,  $C_m^n$  represents the binomial coefficients. All other coefficients are listed in Appendix B for convenience, and  $R_1$ ,  $R_2$  and  $R_3$  are defined as

$$R_1 = \max\left\{\frac{\sqrt{6}}{2}, \frac{\sqrt{2}\kappa_-}{\kappa}\right\}, \quad R_2 = \max\left\{\frac{\sqrt{6}}{2}, \frac{\sqrt{2}}{\kappa}\right\}, \quad R_3 = \max\left\{\frac{\sqrt{6}}{2}, \frac{\sqrt{2}\kappa_+}{\kappa}\right\}. \quad (39)$$

$\Omega(\rho, x)$  denotes the integration of  $F(x, 0)x^\rho$ , which can be expressed as:

$$\begin{aligned} \Omega(\rho, x) &= \frac{3\pi^2}{4} \sum_{m=0}^4 \sum_{n=0}^2 C_4^m C_2^n (-3)^{4-m} (-2)^n I(-16 + 2m + 2n + \rho, 0, x) \\ &\quad + \frac{1}{9} \left(\frac{3}{2}\right)^{\frac{\rho-1}{2}} \sum_{m=0}^2 \sum_{l=0}^2 \sum_{n=0}^{2+l} C_2^m C_{2+l}^n C_2^l (-3)^m (-2)^{4-n} I\left(-\frac{13}{2} + \frac{\rho}{2} + m + n - l, l, \frac{2}{3}x^2\right), \end{aligned} \quad (40)$$

where  $I(a, l, z)$  is defined as

$$I(a, l, z) = \int dz z^a \ln^l(z-1). \quad (41)$$

The analytical expression of  $I(a, l, z)$  depends on the value of  $a$  and  $l$ , which is carefully enumerated in Appendix A.

As for the region  $x < \sqrt{6}/2$ ,  $F(x, 0)$  decays rapidly as  $x$  decreases, and hence the contribution is relatively small on  $\kappa < 2/\sqrt{3}$ , where the peak of  $\mathcal{P}_{\mathcal{R}}(q)$  has not entered this region. In this region,  $F(x, y)$  reduces to

$$F(x, y) = \frac{3(1-2x^2)^2(x^2+y^2-3)^4}{4(x-y)^8(x+y)^8} \left( \ln \frac{3-2y^2}{3-2x^2} + \frac{2(x^2-y^2)}{x^2+y^2-3} \right)^2. \quad (42)$$

We will take the leading order of  $x \rightarrow (\sqrt{6}/2)_-$ ,  $v \rightarrow 0$  and  $x \rightarrow \sqrt{2}/2$  respectively for different areas and add them up.

Firstly for  $x \rightarrow (\sqrt{6}/2)_-$ , we take the expansion on  $(x - \sqrt{6}/2)$  to the constant order and  $y$  to the second order:

$$F(x, y) \approx \frac{16}{27} \left(1 + \frac{8}{3}y^2\right) \ln^2 \left[ \frac{4e^2}{\sqrt{6}} \left(x - \frac{\sqrt{6}}{2}\right) \right]. \quad (43)$$

We perform the integration from the zero point of the expansion at  $x = (\sqrt{6}/2)(1 - (2e^2)^{-1})$ . The width on  $x$  direction is  $< 10^{-1}$ , and it is not until the width shrink to  $10^{-2}$  that the value is comparable with the  $\pi^2$  term in Eq. (28) at  $x = \sqrt{6}/2$ . As a consequence, the power spectrum can be treated as constant of  $x$  if  $\alpha, \beta \leq 10$ :

$$\mathcal{P}_{\mathcal{R}}\left(\frac{x+y}{\sqrt{2}}\kappa\right) \mathcal{P}_{\mathcal{R}}\left(\frac{x-y}{\sqrt{2}}\kappa\right) \approx \mathcal{P}_{\mathcal{R}}^2\left(\frac{\sqrt{3}}{2}\kappa\right) \exp\left\{-\frac{\gamma(\sqrt{3}\kappa/2)}{3/2}y^2\right\}, \quad (44)$$

where  $\gamma(q)$  is defined in Eq. (32). Similarly as Eq. (31), the contribution from this part can be obtained:

$$\begin{aligned}\Omega_{\text{GW}}^{\frac{\sqrt{6}}{2}-}(k) &\approx \frac{16}{27} \mathcal{P}_{\mathcal{R}}^2 \left( \frac{\sqrt{3}}{2} \kappa \right) \int_{\frac{\sqrt{6}}{2}(1-\frac{1}{2e^2})}^{\frac{\sqrt{6}}{2}} dx \ln^2 \left[ \frac{4e^2}{\sqrt{6}} \left( x - \frac{\sqrt{6}}{2} \right) \right] \int_{-\frac{1}{\sqrt{2}}}^{\frac{1}{\sqrt{2}}} dy (1-2y^2)^2 \exp \left\{ \frac{4-\gamma(\sqrt{3}\kappa/2)}{3/2} y^2 \right\}, \\ &= \frac{8\sqrt{6}}{27e^2} \mathcal{P}_{\mathcal{R}}^2 \left( \frac{\sqrt{3}}{2} \kappa \right) \bar{Q} \left( \frac{\sqrt{6}}{2}, \frac{\sqrt{3}}{2} \kappa \right).\end{aligned}\quad (45)$$

Then for  $v \rightarrow 0$ , we take the leading order of Eq. (12) on  $v = 0$  and  $u = 1$  for the region  $v < (\sqrt{3}-1)/2$ :

$$\Omega_{\text{GW}}^{v \rightarrow 0}(k) \approx \mathcal{P}_{\mathcal{R}}(\kappa) \int_0^{\frac{\sqrt{3}-1}{2}} dv v \mathcal{P}_{\mathcal{R}}(v\kappa) \int_{-1}^1 d\delta \mathcal{T}(\delta, v), \quad (46)$$

$$\mathcal{T}(\delta, v) \approx \frac{1}{3}(\delta^2 - 1)^2 v^2, \quad (47)$$

where  $\delta$  is defined by  $u = 1 + v\delta$ . The integration can be done directly:

$$\Omega_{\text{GW}}^{v \rightarrow 0}(k) \approx \frac{32(\alpha + \beta)}{45\beta(\alpha + 4)(\sqrt{3} + 1)^{\alpha+4}} A \mathcal{P}_{\mathcal{R}}(\kappa) \kappa^\alpha {}_2F_1 \left( 1, \frac{\alpha + 4}{\alpha + \beta}; \frac{\alpha + 4}{\alpha + \beta} + 1; -\frac{\lambda \kappa^{\alpha+\beta}}{(\sqrt{3} + 1)^{\alpha+\beta}} \right), \quad (48)$$

where  ${}_2F_1$  is the hypergeometric function. The result has been doubled considering the identical region  $u < (\sqrt{3}-1)/2$ .

Finally, we take the leading order of  $F(x, y)$  in Eq. (42) on  $x = 1/\sqrt{2}$  and the remaining integral reduces to

$$\Omega_{\text{GW}}^{\frac{\sqrt{2}}{2}+}(k) \approx 2400(2 + 5 \ln(2/3))^2 \int_{\frac{1}{\sqrt{2}}}^{\frac{\sqrt{6}}{2}} dx \left( x - \frac{1}{\sqrt{2}} \right)^2 Q(x, q) \mathcal{P}_{\mathcal{R}}^2(q), \quad (49)$$

$$Q(x, q) \approx 2 \int_0^{x+\frac{1-\sqrt{3}}{\sqrt{2}}} dy \exp \left( -\frac{\alpha\beta}{x^2} y^2 \right) \approx \begin{cases} 2x + \sqrt{2} - \sqrt{6} & \text{for } \alpha\beta \leq 3, \\ x \sqrt{\pi/(\alpha\beta)} \text{erf}(1) & \text{for } \alpha\beta > 3. \end{cases} \quad (50)$$

In the last step, we have neglected the  $y^2$  order if  $\alpha\beta \leq 3$ , which means the peak width on  $y$  direction do not enter this region. As for the case  $\alpha\beta > 3$ , we count in a single width on  $y$  direction and hence the result of  $\Omega_{\text{GW}}$  in this region is that

$$\begin{aligned}\Omega_{\text{GW}}^{\frac{\sqrt{2}}{2}+}(k) &\approx \frac{C_\kappa}{2} \sum_{m=0}^2 \left( -\sqrt{2} \right)^m C_2^m \\ &\times \begin{cases} \left( 2I_1(p, \alpha + \beta, 2\alpha + m + 1, x) + (\sqrt{2} - \sqrt{6}) I_1(p, \alpha + \beta, 2\alpha + m, x) \right) \Big|_{\frac{1}{\sqrt{2}}}^{\frac{\sqrt{6}}{2}} & \text{for } \alpha\beta \leq 3, \\ \sqrt{\pi/(\alpha\beta)} \text{erf}(1) I_1(p, \alpha + \beta, 2\alpha + m + 1, x) \Big|_{\frac{1}{\sqrt{2}}}^{\frac{\sqrt{6}}{2}} & \text{for } \alpha\beta > 3. \end{cases}\end{aligned}\quad (51)$$

$$p = \lambda \left( \frac{\kappa}{\sqrt{2}} \right)^{\alpha+\beta}, \quad C_\kappa = 2400(2 + 5 \ln(2/3))^2 2^{-\alpha} A^2 (1 + \lambda)^2 \kappa^{2\alpha}, \quad (52)$$

$$I_1(p, q, r, x) = \int dx \frac{x^r}{(p x^q + 1)^2} = \frac{x^{r+1}}{r+1} {}_2F_1 \left( 2, \frac{r+1}{q}; \frac{r+1}{q} + 1; -p x^q \right). \quad (53)$$

The total contribution of  $x < \sqrt{6}/2$  is the sum of Eqs. (45) (48) and (51), while the parameters are also relevant to Eq. (31):

$$\Omega_{\text{GW}}^{x < \frac{\sqrt{6}}{2}}(k) \approx \Omega_{\text{GW}}^{\frac{\sqrt{6}}{2}-}(k) + \Omega_{\text{GW}}^{\frac{\sqrt{2}}{2}+}(k) + \Omega_{\text{GW}}^{v \rightarrow 0}(k), \quad (54)$$

and the complete  $\Omega_{\text{GW}}(k)$  induced by a broken power-law power spectrum is the combination of the results in Eq. (38a) and Eq. (54):

**Main result:**

$$\Omega_{\text{GW}}(k) = \Omega_{\text{GW}}^{x > \frac{\sqrt{6}}{2}}(k) + \Omega_{\text{GW}}^{x < \frac{\sqrt{6}}{2}}(k). \quad (55)$$



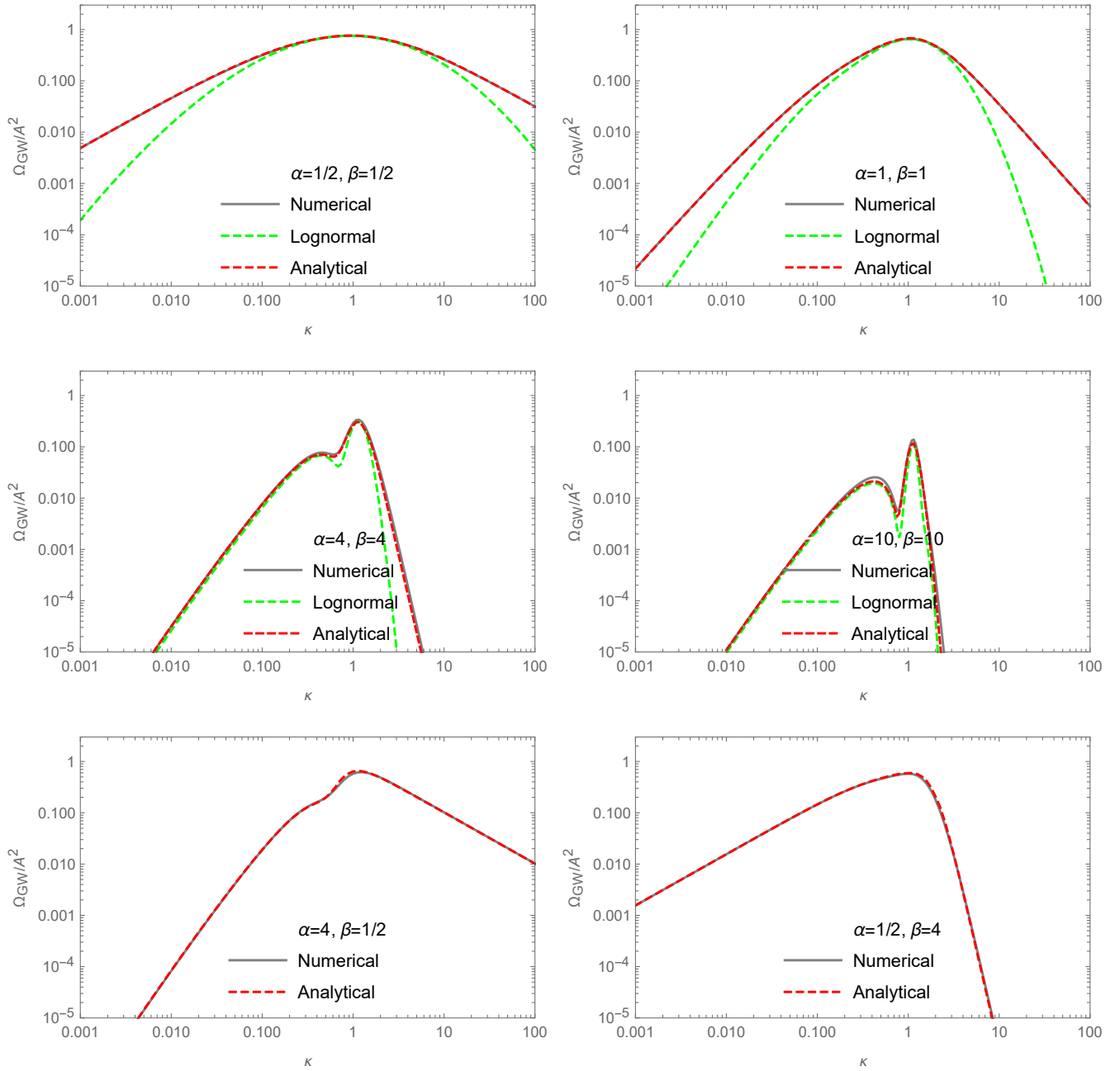


FIG. 1. The analytical results of the normalized  $\Omega_{\text{GW}}$  (where we divide it by  $A^2$ ) generated by broken power-law spectrum as a function of  $\kappa = k/k_*$  together with the numeric results for different values of  $\alpha$  and  $\beta$ . We also show the normalized  $\Omega_{\text{GW}}$  generated by log-normal power spectrum which is characterized in Eq. (22) with  $\Delta = \alpha^{-1}$ .

Eq. (55) is our main result and readers can refer back to the intermediate results as needed. The relevant parameters are listed in Appendix B for a quick approach. The analytical result is compared to the numerical result in Fig. 1.

Furthermore, it is also of vital importance to work out the asymptotic behavior of  $\Omega_{\text{GW}}(k)$  to show a straightforward feature. Firstly for the case  $\kappa < \sqrt{2}\kappa_- \times 10^{-1}$ , the peak of  $\mathcal{P}_{\mathcal{R}}$  lies entirely on  $x > 10$  where the leading order of  $x \rightarrow +\infty$  is a good approximation of  $F(x, y)$ . In this circumstance, the leading order of Eq. (41) is given by:

$$I(a, l, z \gg 1) \approx \int dz z^a \ln^l z = \begin{cases} \frac{z^{a+1}}{a+1} \ln^l z \sum_{j=0}^l \frac{\Gamma(l+1)}{\Gamma(l+1-j)} (-1)^j (1+a)^{-j} \ln^{-j} z, & \text{for } a \neq -1; \\ \frac{1}{l+1} \ln^{l+1} z, & \text{for } a = -1. \end{cases} \quad (56)$$

The overall factor in the case  $a \neq -1$  is the leading order of  $\ln z$ . Both circumstances have a log-dependent  $z^{a+1}$  feature while the leading order of  $\ln z$  is different. Hence the leading order of Eq. (40) is that:

$$\begin{aligned} \Omega(\rho, x \gg 1) &\approx 3\pi^2 I(-4 + \rho, 0, x) + \left(\frac{3}{2}\right)^{\frac{\rho-1}{2}} \sum_{l=0}^2 C_2^l (-2)^{2-l} I\left(-\frac{5}{2} + \frac{\rho}{2}, l, \frac{2}{3}x^2\right), \\ &= \begin{cases} 12 \frac{x^{\rho-3}}{\rho-3} \left[ \frac{\pi^2}{4} + \frac{1}{(\rho-3)^2} + \ln^2 \left( \sqrt{\frac{2}{3}} e^{\frac{\rho-2}{3}} x \right) \right] & \text{for } \rho \neq 3, \\ 3\pi^2 \ln x + 4 \ln^3 \left( \sqrt{\frac{2}{3}} e^{-1} x \right) & \text{for } \rho = 3. \end{cases} \end{aligned} \quad (57)$$

The result roughly shows a  $x^{\rho-3}$  feature, but the dependence of  $\ln x$  is different for  $\rho = 3$ . We consider the contribution from the region  $q > \kappa_-$  first. For the case  $\alpha\beta \leq 6$ , we look up to Eq. (38a) and the leading order of each part on  $q > \kappa_-$  is that:

$$\Omega_{\text{GW}}^{\kappa_- < q < 1}(k) \approx A^2 \frac{8\sqrt{2}}{15} \left( \Omega(0, x) + d_2 \sum_{j=0}^2 C_2^j (-1)^j \left( \frac{\kappa}{\sqrt{2}} \right)^{j\beta} \Omega(j\beta, x) \right) \Big|_{\frac{\sqrt{2}\kappa_-}{\kappa}}^{\frac{\sqrt{2}}{\kappa}}, \quad (58)$$

$$\Omega_{\text{GW}}^{1 < q < \kappa_+}(k) \approx A^2 \frac{8\sqrt{2}}{15} \left( \Omega(0, x) + d_3 \sum_{j=0}^2 C_2^j (-1)^j \left( \frac{\kappa}{\sqrt{2}} \right)^{-j\alpha} \Omega(-j\alpha, x) \right) \Big|_{\frac{\sqrt{2}}{\kappa}}^{\frac{\sqrt{2}\kappa_+}{\kappa}}, \quad (59)$$

$$\Omega_{\text{GW}}^{q > \kappa_+}(k) \approx A^2 (1 + \lambda^{-1})^2 \frac{8\sqrt{2}}{15} \sum_{j=0}^2 C_2^j d_4^j \left( \frac{\kappa}{\sqrt{2}} \right)^{-2\beta - j(\alpha + \beta)} \Omega(-2\beta - j(\alpha + \beta), x) \Big|_{\frac{\sqrt{2}\kappa_+}{\kappa}}^{+\infty}. \quad (60)$$

For each part, the asymptotic behavior is determined by the factor with the same form that

$$\left( \frac{\kappa}{\sqrt{2}} \right)^\rho \Omega(\rho, x) \Big|_{\frac{\sqrt{2}\kappa_i}{\kappa}}^{\frac{\sqrt{2}\kappa_j}{\kappa}} \approx \begin{cases} \frac{3\sqrt{2}}{\rho-3} \left( \kappa_j^{\rho-3} - \kappa_i^{\rho-3} \right) \kappa^3 [(\ln \kappa + B_1)^2 + B_2], & \text{for } \rho \neq 3; \\ 3\sqrt{2} \ln \frac{\kappa_j}{\kappa_i} \kappa^3 [(\ln \kappa + B_1)^2 + B_2], & \text{for } \rho = 3. \end{cases} \quad (61)$$

$$B_1 = \begin{cases} \ln \frac{\sqrt{3}}{2\sqrt{\kappa_i \kappa_j}} + \frac{\rho-2}{\rho-3} - \frac{1}{2} \frac{\kappa_j^{\rho-3} + \kappa_i^{\rho-3}}{\kappa_j^{\rho-3} - \kappa_i^{\rho-3}} \ln \frac{\kappa_j}{\kappa_i} & \text{for } \rho \neq 3, \\ \ln \frac{\sqrt{3}}{2\sqrt{\kappa_i \kappa_j}} + 1 & \text{for } \rho = 3; \end{cases} \quad (62)$$

$$B_2 = \begin{cases} \frac{\pi^2}{4} + \frac{1}{(\rho-3)^2} - \frac{\kappa_j^{\rho-3} \kappa_i^{\rho-3}}{(\kappa_j^{\rho-3} - \kappa_i^{\rho-3})^2} \ln^2 \frac{\kappa_j}{\kappa_i}, & \text{for } \rho \neq 3, \\ \frac{\pi^2}{4} + \frac{1}{12} \ln^2 \frac{\kappa_j}{\kappa_i} & \text{for } \rho = 3. \end{cases} \quad (63)$$

In both cases the factor has a  $\kappa^3 [(\ln \kappa + B_1)^2 + B_2]$  feature. As the sum of Eqs. (58)-(60) keeps the form, we obtain a familiar  $\kappa^3 \ln^2 \kappa$  feature if we keep the leading order of  $\ln \kappa$ , which accords with the result in [37].

Then for  $\alpha\beta > 6$ , the results simply reduce to the results in Eqs. (58)-(60) if it is satisfied that  $\Delta_\kappa \gg 1$  or

Model	Range of $\kappa$	IR Behavior	Dominant Term
$\alpha < 3/2$	$\kappa < \sqrt{2}\kappa_- \times 10^{-1}$	$\kappa^{2\alpha}$	$\kappa^{2\alpha}\Omega(\rho, \sqrt{6}/2)$
$\alpha = 3/2$	$\kappa < \sqrt{2}\kappa_- \times 10^{-1}$	$\kappa^3 \ln^3 \kappa$	$(\kappa/\sqrt{2})^\rho \Omega(\rho, \sqrt{2}\kappa_-/\kappa)$
$\alpha > 3/2$	$\kappa < \sqrt{2}\kappa_- \times 10^{-1}, \kappa \ll \sqrt{10}(\alpha\beta)^{-1/2}$	$\kappa^3 \ln^2 \kappa$	$(\kappa/\sqrt{2})^\rho \Omega(\rho, \sqrt{2}\kappa_i/\kappa)$
$\alpha, \beta \gg 20$	$\sqrt{10}(\alpha\beta)^{-1/2} \ll \kappa < \sqrt{2}\kappa_- \times 10^{-1}$	$\kappa^2 \ln^2 \kappa$	$(\kappa/\sqrt{2})^{\rho-1} \Omega(\rho, \sqrt{2}\kappa_i/\kappa)$

TABLE I. Different IR behavior in different parameter ranges. Properties of the dominant terms are given in Eq. (61), where  $\kappa_i$  includes  $\kappa_-$ , 1,  $\kappa_+$  and  $+\infty$ .

approximately  $\kappa^2(\alpha\beta - 4) \ll 10$ , while another limit  $\kappa^2(\alpha\beta - 4) \gg 10$  gives a different behavior that

$$\Omega_{\text{GW}}^{\kappa_- < q < 1}(k) \approx A^2 \frac{\sqrt{\pi}}{\sqrt{\alpha\beta - 4}} \left( \Omega(1, x) + d_2 \sum_{j=0}^2 C_2^j (-1)^j \left( \frac{\kappa}{\sqrt{2}} \right)^{j\beta} \Omega(1 + j\beta, x) \right) \Bigg|_{\frac{\sqrt{2}\kappa_-}{\kappa}}^{\frac{\sqrt{2}}{\kappa}}, \quad (64)$$

$$\Omega_{\text{GW}}^{1 < q < \kappa_+}(k) \approx A^2 \frac{\sqrt{\pi}}{\sqrt{\alpha\beta - 4}} \left( \Omega(1, x) + d_3 \sum_{j=0}^2 C_2^j (-1)^j \left( \frac{\kappa}{\sqrt{2}} \right)^{-j\alpha} \Omega(1 - j\alpha, x) \right) \Bigg|_{\frac{\sqrt{2}}{\kappa}}^{\frac{\sqrt{2}\kappa_+}{\kappa}}, \quad (65)$$

$$\Omega_{\text{GW}}^{q > \kappa_+}(k) \approx A^2 (1 + \lambda^{-1})^2 \kappa_+^5 \frac{\sqrt{\pi}}{\sqrt{\alpha\beta - 4}} \sum_{j=0}^2 C_2^j d_4^j \left( \frac{\kappa}{\sqrt{2}} \right)^{-5-2\beta-j(\alpha+\beta)} \Omega(-4 - 2\beta - j(\alpha + \beta), x) \Bigg|_{\frac{\sqrt{2}\kappa_+}{\kappa}}^{+\infty}, \quad (66)$$

where we notice that the feature reduce to  $\kappa^2 \ln^2 \kappa$  since the corresponding factor reduce to  $(\kappa/\sqrt{2})^{\rho-1} \Omega(\rho, x)$  compared with Eq. (61). Also, this feature accords with the result in [37] for a power spectrum with a finite but extremely small width. In the broken power-law case, this approximately means  $\alpha, \beta \gg 20$  and  $\kappa \gg \sqrt{10}(\alpha\beta)^{-1/2}$ .

The remaining  $q < \kappa_-$  part is quite different in the integrated area, and the  $\kappa \ll 1$  limit gives

$$\begin{aligned} \Omega_{\text{GW}}^{q < \kappa_-}(k) \approx & A^2 (1 + \lambda)^2 \left[ \sum_{j=0}^2 C_2^j d_1^j a_0 \left( \frac{\kappa}{\sqrt{2}} \right)^{2\alpha+j(\alpha+\beta)} \Omega(2\alpha + j(\alpha + \beta), \frac{\sqrt{2}\kappa_-}{\kappa}) \right. \\ & \left. - \left( \frac{\kappa}{\sqrt{2}} \right)^{2\alpha} \sum_{\rho_i=0, -2} a_{\rho_i} \Omega(\rho_i + 2\alpha, \frac{\sqrt{6}}{2}) \right]. \end{aligned} \quad (67)$$

Given that  $a_0$  is nearly constant when  $\kappa^2(\alpha\beta - 4) \ll 10$  while proportional to  $\kappa^{-1}$  when  $\kappa^2(\alpha\beta - 4) \gg 10$ , the first  $\Omega(\rho, x)$  term shows a similar  $\kappa^3 \ln^2 \kappa$  or  $\kappa^2 \ln^2 \kappa$  feature. However,  $a_{-2}$  is constant in both cases and hence the second  $\Omega(\rho, x)$  term contributes to a  $\kappa^{2\alpha}$  term. Consequently, this part takes over the IR region if  $\alpha < 3/2$ , which is a significant feature of a power-law power spectrum. When considering  $\alpha = 3/2$  as a critical case, we find the first  $\Omega(\rho, x)$  term behaves as  $\kappa^3 \ln^3 \kappa$  as shown in Eq. (57) which accords with the result in [89]. To summarize, different IR behaviors are listed in Table I.

As for the UV region of  $\Omega_{\text{GW}}$ , only the  $q > \kappa_+$  part is non zero in Eq. (38a), of which the leading order is that

$$\Omega_{\text{GW}}^{q > \kappa_+}(k) \approx A^2 (1 + \lambda^{-1})^2 \left( \frac{\kappa}{\sqrt{2}} \right)^{-2\beta} \sum_{\rho_i=0, -2} c_{\rho_i} \Omega(\rho_i - 2\beta, x) \Bigg|_{\sqrt{6}/2}^{+\infty}, \quad (68)$$

which is proportional to  $\kappa^{-2\beta}$ . The contribution from Eq. (54) is that

$$\Omega_{\text{GW}}^{\frac{\sqrt{6}}{2}-}(k) \approx A^2 \frac{128(1+\lambda^{-1})^2}{135\sqrt{3}e^2} \left(1 + \frac{4+\beta}{21}\right) \left(\frac{3}{4}\right)^{-\beta} \kappa^{-2\beta}; \quad (69)$$

$$\Omega_{\text{GW}}^{v \rightarrow 0}(k) \approx A^2 \frac{32}{45\alpha} (\lambda^{-1} + 1) \times \begin{cases} \left[ (\sqrt{3}+1)^{-4+\beta} \frac{\alpha+\beta}{4-\beta} \kappa^{-2\beta} + \pi \lambda^{\frac{\beta-4}{\alpha+\beta}} \csc\left(\frac{\pi(\alpha+4)}{\alpha+\beta}\right) \kappa^{-\beta-4} \right] & \text{for } \beta \neq 4, \\ (\alpha+4)\kappa^{-8} \left( \ln \kappa - \ln(\sqrt{3}+1) + \frac{1}{\alpha+4} \ln \frac{\alpha}{4} \right) & \text{for } \beta = 4; \end{cases} \quad (70)$$

$$\Omega_{\text{GW}}^{\frac{\sqrt{2}}{2}+}(k) \approx A^2 75 \cdot 2^{\beta+5} (2 + 5 \ln(2/3))^2 (1 + \lambda^{-1})^2 \kappa^{-2\beta} \sum_{m=0}^2 (-1)^m 2^{m/2} C_2^m \times \begin{cases} \left( \frac{x^{-2\beta+m+2}}{-2\beta+m+2} + \frac{\sqrt{2}-\sqrt{6}}{2} \frac{x^{-2\beta+m+1}}{-2\beta+m+1} \right) \Big|_{\sqrt{2}/2}^{\sqrt{6}/2} & \text{for } \alpha\beta \leq 3, \\ \frac{\text{erf}(1)\sqrt{\pi}}{2\sqrt{\alpha\beta}} \frac{x^{-2\beta+m+2}}{-2\beta+m+2} \Big|_{\sqrt{2}/2}^{\sqrt{6}/2} & \text{for } \alpha\beta > 3. \end{cases} \quad (71)$$

The contribution from Eq. (70) has a  $\kappa^{-4-\beta}$  term while other parts are proportional to  $\kappa^{-2\beta}$ , which are contributions from the UV tail of the power spectrum on  $q > \kappa_+$ . In the critical case  $\beta = 4$ , we find a different  $\kappa^{-8} \ln \kappa$  feature in Eq. (70). The approximation is valid if the peak of power spectrum appears only in  $\Omega_{\text{GW}}^{v \rightarrow 0}(k)$  and this roughly means  $\kappa > (\sqrt{2} + \sqrt{6})\kappa_+$ . The results in Eqs. (68)-(71) can be extended to a general case of a power-law UV tail except for the coefficients of  $\kappa^{-4-\beta}$  and  $\kappa^{-8} \ln \kappa$  in Eq. (70) which is also given by the near-peak behavior.

#### IV. CONCLUSION

In this paper, we have derived an analytical result for the energy spectrum  $\Omega_{\text{GW}}(k)$  of SIGWs induced by the scalar perturbations with a broken power-law power spectrum with high precision. These scalar perturbations can be generated from single-field inflation, and we consider the SIGWs produced during the RD era, during which PBHs may have formed and now constitute a significant fraction of dark matter. The shape of  $\Omega_{\text{GW}}(k)$  is sensitive to the form of the scalar power spectrum, particularly to the decaying power indices  $\alpha$  and  $\beta$  for IR and UV regions respectively, and is proportional to the square of the amplitude,  $A$ . The complete analytical result is given in Eq. (55). Moreover, our result can be used as a near-peak approximation in more general cases since the broken power-law power spectrum has abundant near-peak feature.

To facilitate the calculation, we separate the power-law tails of  $\mathcal{P}_{\mathcal{R}}$  and reconstruct the near-peak feature as shown in Eq. (20). Considering the transfer function part of  $\Omega_{\text{GW}}(k)$ , or  $F(x, y)$  in Eq. (27), we separate the integral from the resonant peak of the source term at  $x = \sqrt{6}/2$ , corresponding physically to  $|\mathbf{k} - \mathbf{p}| + p = \sqrt{3}k$ . The region  $x > \sqrt{6}/2$  is the main contribution of the integral, and contribute to the detailed shape of  $\Omega_{\text{GW}}$ . The contribution of this part is given in Eq. (38a), where the contributions from different regions of  $\mathcal{P}_{\mathcal{R}}$  are given separately in Eqs. (38b)-(38e). On the other region  $x < \sqrt{6}/2$ , the transfer function decays rapidly and the result is given in Eq. (54).

As for the UV and IR regions of  $\Omega_{\text{GW}}$ , our results are compatible with the previous works. The results for the IR case are given in Eqs. (58)-(67) and listed in Table I, where we see a typical  $\kappa^3 \ln^2 \kappa$  feature which was found in SIGWs induced by a general peaked power spectrum, and a  $\kappa^{2\alpha}$  term which is similar to the result of a power-law power spectrum. We also obtain a different  $\kappa^3 \ln^3 \kappa$  feature for the critical case  $\alpha = 3/2$ . The unique log-dependent scaling in the infrared region could be a smoking gun in searching for SIGWs. The behavior in UV region is given in Eqs. (68)-(71). The results on most areas are proportional to  $\kappa^{-2\beta}$  while the  $x^2 - y^2 \ll 1$  region has a  $\kappa^{-4-\beta}$  term. For the critical case  $\beta = 4$ , we also obtain a different  $\kappa^{-8} \ln \kappa$  feature.

As for the near-peak case, the calculation is quite different for  $\alpha\beta \leq 6$  and  $\alpha\beta > 6$ , which distinguishes whether the width of  $\mathcal{P}_{\mathcal{R}}(\kappa)$  enters the integral on  $y$  direction when resonating with the mean peak of  $F(x, y)$  at  $x = \sqrt{6}/2$ . In the case  $\alpha\beta > 6$ , an overall factor which has a transition from constant to  $\kappa^{-1}$  is found in Eq. (36). Moreover, if  $\alpha, \beta \gg 20$ , the width of the peak on  $y$  direction does not leave the integral until  $\kappa < \sqrt{2}\kappa_-/10$  and  $\Omega_{\text{GW}}(k)$  enters the IR region. In this case, an extra transition from  $\kappa^3 \ln^2 \kappa$  in the far IR region to  $\kappa^2 \ln^2 \kappa$  in the near IR region occurs when  $\kappa \approx \sqrt{10}(\alpha\beta)^{-1/2}$ . The  $\kappa^2 \ln^2 \kappa$  feature is listed in Eqs. (64)-(66) which is a typical feature induced by a delta function power spectrum. This transition is also found for both a cut-off peak and a log-normal peak in the power spectrum.

In this work, we have assumed that the scalar fluctuations are Gaussian, while non-Gaussianities are also important since the influence on PBH abundance and the SIGW spectrum can be significantly different. Moreover, we have only considered the tensor perturbations to the second order of scalar perturbations, while higher-order perturbations might lead to detectable signatures if the amplitude of the scalar power spectrum is pretty large. The topics above may cause detectable deformation but the analytical results for more general cases still remain to be solved.

*Acknowledgments.* This work is supported by the National Key Research and Development Program of China Grant No.2020YFC2201502, grants from NSFC (grant No. 11991052, 12250010), Key Research Program of Frontier Sciences, CAS, Grant NO. ZDBS-LY-7009. C.Y. acknowledge the financial support provided under the European Union’s H2020 ERC Advanced Grant “Black holes: gravitational engines of discovery” grant agreement no. Gravitas–101052587. Views and opinions expressed are however those of the author only and do not necessarily reflect those of the European Union or the European Research Council. Neither the European Union nor the granting authority can be held responsible for them. We acknowledge support from the Villum Investigator program supported by the VILLUM Foundation (grant no. VIL37766) and the DNRF Chair program (grant no. DNRF162) by the Danish National Research Foundation.

### Appendix A: analytical expressions of integrals

In this section, we give the analytical expressions of the integral  $I(a, l, z)$  defined in Eq. (41), where the case containing  $m \in \mathbb{N}$  and  $m > 1$  is to cover the singularity at  $a = -m$ .

$$I(a, l, z) = \int z^a \ln^l(z-1) dz, \quad (\text{A1a})$$

$$I(a, 2, z) = 2(z-1) {}_4F_3(1, 1, 1, -a; 2, 2, 2; 1-z) - 2(z-1) \ln(z-1) {}_3F_2(1, 1, -a; 2, 2; 1-z) + \frac{(z^{a+1} - 1) \ln^2(z-1)}{a+1}, \quad (\text{A1b})$$

$$I(-1, 2, z) = -2\text{Li}_3(1-z) + 2\text{Li}_2(1-z) \ln(z-1) + \ln(z) \ln^2(z-1), \quad (\text{A1c})$$

$$I(a, 1, z) = \frac{z^{a+2} \text{Re} [ {}_2F_1(1, a+2; a+3; z) ]}{(a+1)(a+2)} + \frac{z^{a+1} \ln(z-1)}{a+1}, \quad (\text{A1d})$$

$$I(-m, 1, z) = \frac{1}{m-1} (\ln(z-1) - \ln(z)) + \sum_{l=1}^{m-2} \frac{z^{-(-l+m-1)}}{-l+m-1} - z^{1-m} \ln(z-1),$$

$$= \frac{z^{1-m}}{1-m} (\Phi_L(z^{-1}, 1, m-1) + \ln(z-1)), \quad (\text{A1e})$$

$$I(-1, 1, z) = \text{Li}_2(1-z) + \ln(z-1) \ln(z), \quad (\text{A1f})$$

$$I(a, 0, z) = \frac{z^{a+1}}{a+1}, \quad I(-1, 0, z) = \ln z, \quad (\text{A1g})$$

where  ${}_pF_q$  is the hypergeometric function,  $\text{Li}_n(x)$  is the polylog function and  $\Phi_L$  is Lerch’s transcendental function. The limits of the functions above are not trivial, so we give the results directly:

$$\lim_{z \rightarrow 1^+} I(a, 2, z) = 0, \quad (\text{A2a})$$

$$\lim_{z \rightarrow +\infty} I(a, 2, z) = -\frac{6(H_{-a-2})^2 + 6\psi^{(1)}(-a-1) + \pi^2}{6a+6}, \quad (\text{A2b})$$

$$\lim_{z \rightarrow 1^+} I(a, 1, z) = -\frac{H_{a+1}}{a+1}, \quad (\text{A2c})$$

$$\lim_{z \rightarrow +\infty} I(a, 1, z) = \frac{\pi \cot(\pi a)}{a+1}, \quad (\text{A2d})$$

$$\lim_{z \rightarrow 1^+} I(-m, 1, z) = \frac{H_{m-2}}{m-1}, \quad (\text{A2e})$$

$$\lim_{z \rightarrow +\infty} I(-m, 1, z) = 0, \quad (\text{A2f})$$

$$\lim_{z \rightarrow 1^+} I(-1, 1, z) = 0. \quad (\text{A2g})$$

$H_n$  is the harmonic number and  $\psi^{(1)}$  is the derivative of polygamma function. It is also useful to exclude Eqs. (A2a)-(A2g) from Eqs. (A1b)-(A1g) when considering the asymptotic behavior, since the  $I(a, l, z \gg 1)$  will have a log-dependent  $z^{a+1}$  feature automatically and the result is the same as Eq. (56).

### Appendix B: parameters

In this section, we list the coefficients used in Sec. III B.

Firstly for those relevant to the segment of the scalar power spectrum which is derived in Sec. III A:

$$\mathcal{P}_{\mathcal{R}}(q) = A \frac{\alpha + \beta}{\beta q^{-\alpha} + \alpha q^{\beta}}, \quad (\text{B1})$$

$$\kappa_- = (1 + \lambda)^{-1/\alpha}, \quad \kappa_+ = (1 + \lambda^{-1})^{1/\beta}, \quad \lambda = \alpha/\beta, \quad (\text{B2})$$

$$d_1 = \frac{\mathcal{P}_{\mathcal{R}}(\kappa_-) - 1}{\kappa_-^{\alpha+\beta}(1 + \lambda)}, \quad d_2 = \frac{\mathcal{P}_{\mathcal{R}}^2(\kappa_-) - 1}{(\kappa_-^{\beta} - 1)^2}, \quad d_3 = \frac{\mathcal{P}_{\mathcal{R}}^2(\kappa_+) - 1}{(\kappa_+^{-\alpha} - 1)^2}, \quad d_4 = \frac{\mathcal{P}_{\mathcal{R}}(\kappa_+) - 1}{(1 + \lambda^{-1})} \kappa_+^{\alpha+\beta}. \quad (\text{B3})$$

Then for the coefficients relevant to the integration on  $y$  direction,

$$\bar{Q}(x, q) = \frac{\sqrt{\pi} (c^2 + 2c + 3) \operatorname{erfi}(\sqrt{c/2})}{c^{5/2}} - \frac{\sqrt{2}(c + 3)e^{c/2}}{c^2}, \quad (\text{B4})$$

$$c(x, q) = \frac{4 - \gamma(q)}{x^2}, \quad \gamma(q) = \alpha\beta \frac{\beta + (\alpha^2 + 2\alpha\beta + \alpha + (\beta - 1)\beta) q^{\alpha+\beta} - \alpha q^{2(\alpha+\beta)}}{(\beta + \alpha q^{\alpha+\beta})^2}, \quad (\text{B5})$$

$$Q_c \left( \frac{\sqrt{2}\kappa_{\pm}}{\kappa}, \kappa \right) = \begin{cases} \frac{8\sqrt{2}}{15} \left( 1 + \frac{4 - \alpha\beta}{14} \frac{\kappa^2}{2\kappa_{\pm}} \right) & \text{for } \alpha\beta \leq 6, \\ \frac{1}{\kappa} \sqrt{\frac{2\pi}{(\alpha\beta - 4)(\Delta_{\kappa} + 1)}} \frac{\Delta_{\kappa} + \kappa_{\pm}}{\Delta_{\kappa} + 1} & \text{for } \alpha\beta > 6, \end{cases} \quad (\text{B6})$$

where  $q = \kappa x / \sqrt{2}$  and  $\Delta_{\kappa}$  is defined as

$$\Delta_{\kappa} = \frac{225}{128} \frac{2\pi}{\kappa^2(\alpha\beta - 4)}. \quad (\text{B7})$$

For the contribution from the region  $\kappa_- \leq q \leq \kappa_+$ , the relevant coefficients in Eq. (38c) and Eq. (38d) are that

$$(\rho_i, b_{\rho_i}) \in \begin{cases} \left\{ \left( 0, \frac{8\sqrt{2}}{15} \right), \left( -2, \frac{b_0}{14} (4 - \alpha\beta) \right) \right\}, & \text{for } \alpha\beta \leq 6; \\ \left\{ \left( 0, \sqrt{\frac{2\pi}{(\alpha\beta - 4)(\Delta_{\kappa} + 1)^{3/2}}} \frac{\kappa^{-1} \Delta_{\kappa}}{(\Delta_{\kappa} + 1)^{3/2}} \right), \left( 1, \sqrt{\frac{\pi}{(\alpha\beta - 4)(\Delta_{\kappa} + 1)^{3/2}}} \frac{1}{(\Delta_{\kappa} + 1)^{3/2}} \right) \right\}, & \text{for } \alpha\beta > 6. \end{cases} \quad (\text{B8})$$

For the region  $q < \kappa_-$ , the relevant coefficients in Eq. (38b) are that

$$(\rho_i, a_{\rho_i}) \in \left\{ \left( 0, Q_c \left( \frac{\sqrt{2}\kappa_-}{\kappa}, \kappa \right) - \left( \frac{\sqrt{2}\kappa_-}{\kappa} \right)^{-2} a_{-2} \right), \left( -2, \frac{Q_c(\sqrt{2}\kappa_-/\kappa, \kappa) - \bar{Q}(\sqrt{6}/2, \sqrt{3}\kappa/2)}{(\sqrt{2}\kappa_-/\kappa)^{-2} - 2/3} \right) \right\}. \quad (\text{B9})$$

For the region  $q > \kappa_+$ , the relevant coefficients in Eq. (38e) are that

$$(\rho_i, c_{\rho_i}) \in \left\{ \left( 0, \frac{8\sqrt{2}}{15} \right), \left( -2, \frac{c_0}{14} (4 + \beta) \right), \left( -4, \left( Q_c \left( \frac{\sqrt{2}\kappa_+}{\kappa}, \kappa \right) - c_0 - c_{-2} \left( \frac{\sqrt{2}\kappa_+}{\kappa} \right)^{-2} \right) \left( \frac{\sqrt{2}\kappa_+}{\kappa} \right)^4 \right) \right\}. \quad (\text{B10})$$

It is also used that for  $\alpha\beta \leq 6$ ,  $c_{-4}$  reduces to that

$$c_{-4} = -\frac{c_0}{14} \beta (1 + \alpha) \left( \frac{\sqrt{2}\kappa_+}{\kappa} \right)^2. \quad (\text{B11})$$

- 
- [1] Kenji Tomita, “Non-Linear Theory of Gravitational Instability in the Expanding Universe,” *Prog. Theor. Phys.* **37**, 831–846 (1967).
- [2] Sabino Matarrese, Ornella Pantano, and Diego Saez, “A General relativistic approach to the nonlinear evolution of collisionless matter,” *Phys. Rev. D* **47**, 1311–1323 (1993).
- [3] Sabino Matarrese, Ornella Pantano, and Diego Saez, “General relativistic dynamics of irrotational dust: Cosmological implications,” *Phys. Rev. Lett.* **72**, 320–323 (1994), [arXiv:astro-ph/9310036](#).
- [4] Sabino Matarrese, Silvia Mollerach, and Marco Bruni, “Second order perturbations of the Einstein-de Sitter universe,” *Phys. Rev. D* **58**, 043504 (1998), [arXiv:astro-ph/9707278](#).
- [5] Hyerim Noh and Jai-chan Hwang, “Second-order perturbations of the Friedmann world model,” *Phys. Rev. D* **69**, 104011 (2004).
- [6] Carmelita Carbone and Sabino Matarrese, “A Unified treatment of cosmological perturbations from super-horizon to small scales,” *Phys. Rev. D* **71**, 043508 (2005), [arXiv:astro-ph/0407611](#).
- [7] Kouji Nakamura, “Second-order gauge invariant cosmological perturbation theory: Einstein equations in terms of gauge invariant variables,” *Prog. Theor. Phys.* **117**, 17–74 (2007), [arXiv:gr-qc/0605108](#).
- [8] Ryo Saito and Jun’ichi Yokoyama, “Gravitational wave background as a probe of the primordial black hole abundance,” *Phys. Rev. Lett.* **102**, 161101 (2009), [Erratum: *Phys.Rev.Lett.* 107, 069901 (2011)], [arXiv:0812.4339 \[astro-ph\]](#).
- [9] Ryo Saito and Jun’ichi Yokoyama, “Gravitational-Wave Constraints on the Abundance of Primordial Black Holes,” *Prog. Theor. Phys.* **123**, 867–886 (2010), [Erratum: *Prog.Theor.Phys.* 126, 351–352 (2011)], [arXiv:0912.5317 \[astro-ph.CO\]](#).
- [10] Edgar Bugaev and Peter Klimai, “Induced gravitational wave background and primordial black holes,” *Phys. Rev. D* **81**, 023517 (2010), [arXiv:0908.0664 \[astro-ph.CO\]](#).
- [11] Edgar Bugaev and Peter Klimai, “Constraints on the induced gravitational wave background from primordial black holes,” *Phys. Rev. D* **83**, 083521 (2011), [arXiv:1012.4697 \[astro-ph.CO\]](#).
- [12] N. Aghanim *et al.* (Planck), “Planck 2018 results. VI. Cosmological parameters,” *Astron. Astrophys.* **641**, A6 (2020), [Erratum: *Astron.Astrophys.* 652, C4 (2021)], [arXiv:1807.06209 \[astro-ph.CO\]](#).
- [13] Y. Akrami *et al.* (Planck), “Planck 2018 results. X. Constraints on inflation,” *Astron. Astrophys.* **641**, A10 (2020), [arXiv:1807.06211 \[astro-ph.CO\]](#).
- [14] Kishore N. Ananda, Chris Clarkson, and David Wands, “The Cosmological gravitational wave background from primordial density perturbations,” *Phys. Rev. D* **75**, 123518 (2007), [arXiv:gr-qc/0612013](#).
- [15] Daniel Baumann, Paul J. Steinhardt, Keitaro Takahashi, and Kiyotomo Ichiki, “Gravitational Wave Spectrum Induced by Primordial Scalar Perturbations,” *Phys. Rev. D* **76**, 084019 (2007), [arXiv:hep-th/0703290](#).
- [16] Hooshyar Assadullahi and David Wands, “Constraints on primordial density perturbations from induced gravitational waves,” *Phys. Rev. D* **81**, 023527 (2010), [arXiv:0907.4073 \[astro-ph.CO\]](#).
- [17] Keisuke Inomata and Tomohiro Nakama, “Gravitational waves induced by scalar perturbations as probes of the small-scale primordial spectrum,” *Phys. Rev. D* **99**, 043511 (2019), [arXiv:1812.00674 \[astro-ph.CO\]](#).
- [18] Yizhou Lu, Yungui Gong, Zhu Yi, and Fengge Zhang, “Constraints on primordial curvature perturbations from primordial black hole dark matter and secondary gravitational waves,” *JCAP* **12**, 031 (2019), [arXiv:1907.11896 \[gr-qc\]](#).
- [19] Chen Yuan, Zu-Cheng Chen, and Qing-Guo Huang, “Probing primordial–black-hole dark matter with scalar induced gravitational waves,” *Phys. Rev. D* **100**, 081301 (2019), [arXiv:1906.11549 \[astro-ph.CO\]](#).
- [20] Shasvath J. Kapadia, Kanhaiya Lal Pandey, Teruaki Suyama, Shivaraj Kandhasamy, and Parameswaran Ajith, “Search for the Stochastic Gravitational-wave Background Induced by Primordial Curvature Perturbations in LIGO’s Second Observing Run,” *Astrophys. J. Lett.* **910**, L4 (2021), [arXiv:2009.05514 \[gr-qc\]](#).
- [21] H. V. Ragavendra, “Accounting for scalar non-Gaussianity in secondary gravitational waves,” *Phys. Rev. D* **105**, 063533 (2022), [arXiv:2108.04193 \[astro-ph.CO\]](#).
- [22] Matteo Braglia, Xingang Chen, and Dhiraj Kumar Hazra, “Probing Primordial Features with the Stochastic Gravitational Wave Background,” *JCAP* **03**, 005 (2021), [arXiv:2012.05821 \[astro-ph.CO\]](#).
- [23] Lukas T. Witkowski, Guillem Domènech, Jacopo Fumagalli, and Sébastien Renaux-Petel, “Expansion history-dependent oscillations in the scalar-induced gravitational wave background,” *JCAP* **05**, 028 (2022), [arXiv:2110.09480 \[astro-ph.CO\]](#).
- [24] Shyam Balaji, Guillem Domenech, and Joseph Silk, “Induced gravitational waves from slow-roll inflation after an enhancing phase,” *JCAP* **09**, 016 (2022), [arXiv:2205.01696 \[astro-ph.CO\]](#).
- [25] Laila Alabidi, Kazunori Kohri, Misao Sasaki, and Yuuiti Sendouda, “Observable induced gravitational waves from an early matter phase,” *JCAP* **05**, 033 (2013), [arXiv:1303.4519 \[astro-ph.CO\]](#).
- [26] Keisuke Inomata, Kazunori Kohri, Tomohiro Nakama, and Takahiro Terada, “Gravitational Waves Induced by Scalar Perturbations during a Gradual Transition from an Early Matter Era to the Radiation Era,” *JCAP* **10**, 071 (2019), [Erratum: *JCAP* 08, E01 (2023)], [arXiv:1904.12878 \[astro-ph.CO\]](#).
- [27] Keisuke Inomata, Kazunori Kohri, Tomohiro Nakama, and Takahiro Terada, “Enhancement of Gravitational Waves Induced by Scalar Perturbations due to a Sudden Transition from an Early Matter Era to the Radiation Era,” *Phys. Rev. D* **100**, 043532 (2019), [Erratum: *Phys.Rev.D* 108, 049901 (2023)], [arXiv:1904.12879 \[astro-ph.CO\]](#).
- [28] Guillem Domènech, Shi Pi, and Misao Sasaki, “Induced gravitational waves as a probe of thermal history of the universe,”

- JCAP **08**, 017 (2020), [arXiv:2005.12314 \[gr-qc\]](#).
- [29] Ioannis Dalianis and Chris Kouvaris, “Gravitational waves from density perturbations in an early matter domination era,” JCAP **07**, 046 (2021), [arXiv:2012.09255 \[astro-ph.CO\]](#).
- [30] Chengjie Fu, Puxun Wu, and Hongwei Yu, “Scalar induced gravitational waves in inflation with gravitationally enhanced friction,” Phys. Rev. D **101**, 023529 (2020), [arXiv:1912.05927 \[astro-ph.CO\]](#).
- [31] Masahiro Kawasaki, Hiromasa Nakatsuka, and Ippei Obata, “Generation of Primordial Black Holes and Gravitational Waves from Dilaton-Gauge Field Dynamics,” JCAP **05**, 007 (2020), [arXiv:1912.09111 \[astro-ph.CO\]](#).
- [32] José Ramón Espinosa, Davide Racco, and Antonio Riotto, “A Cosmological Signature of the SM Higgs Instability: Gravitational Waves,” JCAP **09**, 012 (2018), [arXiv:1804.07732 \[hep-ph\]](#).
- [33] Kazunori Kohri and Takahiro Terada, “Semianalytic calculation of gravitational wave spectrum nonlinearly induced from primordial curvature perturbations,” Phys. Rev. D **97**, 123532 (2018), [arXiv:1804.08577 \[gr-qc\]](#).
- [34] Guillem Domènech, “Induced gravitational waves in a general cosmological background,” Int. J. Mod. Phys. D **29**, 2050028 (2020), [arXiv:1912.05583 \[gr-qc\]](#).
- [35] Caner Unal, “Imprints of Primordial Non-Gaussianity on Gravitational Wave Spectrum,” Phys. Rev. D **99**, 041301 (2019), [arXiv:1811.09151 \[astro-ph.CO\]](#).
- [36] Atsuhisa Ota, “Induced superhorizon tensor perturbations from anisotropic non-Gaussianity,” Phys. Rev. D **101**, 103511 (2020), [arXiv:2001.00409 \[astro-ph.CO\]](#).
- [37] Chen Yuan, Zu-Cheng Chen, and Qing-Guo Huang, “Log-dependent slope of scalar induced gravitational waves in the infrared regions,” Phys. Rev. D **101**, 043019 (2020), [arXiv:1910.09099 \[astro-ph.CO\]](#).
- [38] Chen Yuan and Qing-Guo Huang, “Gravitational waves induced by the local-type non-Gaussian curvature perturbations,” Phys. Lett. B **821**, 136606 (2021), [arXiv:2007.10686 \[astro-ph.CO\]](#).
- [39] Fengge Zhang, Yungui Gong, Jiong Lin, Yizhou Lu, and Zhu Yi, “Primordial non-Gaussianity from G-inflation,” JCAP **04**, 045 (2021), [arXiv:2012.06960 \[astro-ph.CO\]](#).
- [40] Vicente Atal and Guillem Domènech, “Probing non-Gaussianities with the high frequency tail of induced gravitational waves,” JCAP **06**, 001 (2021), [Erratum: JCAP 10, E01 (2023)], [arXiv:2103.01056 \[astro-ph.CO\]](#).
- [41] Peter Adshead, Kaloian D. Lozanov, and Zachary J. Weiner, “Non-Gaussianity and the induced gravitational wave background,” JCAP **10**, 080 (2021), [arXiv:2105.01659 \[astro-ph.CO\]](#).
- [42] Chen Yuan, De-Shuang Meng, and Qing-Guo Huang, “Full analysis of the scalar-induced gravitational waves for the curvature perturbation with local-type non-Gaussianities,” JCAP **12**, 036 (2023), [arXiv:2308.07155 \[astro-ph.CO\]](#).
- [43] Giacomo Ferrante, Gabriele Franciolini, Antonio Iovino, Junior., and Alfredo Urbano, “Primordial non-Gaussianity up to all orders: Theoretical aspects and implications for primordial black hole models,” Phys. Rev. D **107**, 043520 (2023), [arXiv:2211.01728 \[astro-ph.CO\]](#).
- [44] Nicholas Orlofsky, Aaron Pierce, and James D. Wells, “Inflationary theory and pulsar timing investigations of primordial black holes and gravitational waves,” Phys. Rev. D **95**, 063518 (2017), [arXiv:1612.05279 \[astro-ph.CO\]](#).
- [45] Christian T. Byrnes, Philippa S. Cole, and Subodh P. Patil, “Steepest growth of the power spectrum and primordial black holes,” JCAP **06**, 028 (2019), [arXiv:1811.11158 \[astro-ph.CO\]](#).
- [46] De-Shuang Meng, Chen Yuan, and Qing-Guo Huang, “Primordial black holes generated by the non-minimal spectator field,” Sci. China Phys. Mech. Astron. **66**, 280411 (2023), [arXiv:2212.03577 \[astro-ph.CO\]](#).
- [47] Keisuke Inomata, Masahiro Kawasaki, Kyohei Mukaida, Yuichiro Tada, and Tsutomu T. Yanagida, “Inflationary primordial black holes for the LIGO gravitational wave events and pulsar timing array experiments,” Phys. Rev. D **95**, 123510 (2017), [arXiv:1611.06130 \[astro-ph.CO\]](#).
- [48] Tomohiro Nakama, Joseph Silk, and Marc Kamionkowski, “Stochastic gravitational waves associated with the formation of primordial black holes,” Phys. Rev. D **95**, 043511 (2017), [arXiv:1612.06264 \[astro-ph.CO\]](#).
- [49] Juan Garcia-Bellido, Marco Peloso, and Caner Unal, “Gravitational Wave signatures of inflationary models from Primordial Black Hole Dark Matter,” JCAP **09**, 013 (2017), [arXiv:1707.02441 \[astro-ph.CO\]](#).
- [50] Misao Sasaki, Teruaki Suyama, Takahiro Tanaka, and Shuichiro Yokoyama, “Primordial black holes—perspectives in gravitational wave astronomy,” Class. Quant. Grav. **35**, 063001 (2018), [arXiv:1801.05235 \[astro-ph.CO\]](#).
- [51] Sebastien Clesse, Juan García-Bellido, and Stefano Orani, “Detecting the Stochastic Gravitational Wave Background from Primordial Black Hole Formation,” (2018), [arXiv:1812.11011 \[astro-ph.CO\]](#).
- [52] Keisuke Inomata, Masahiro Kawasaki, Kyohei Mukaida, Takahiro Terada, and Tsutomu T. Yanagida, “Gravitational Wave Production right after a Primordial Black Hole Evaporation,” Phys. Rev. D **101**, 123533 (2020), [arXiv:2003.10455 \[astro-ph.CO\]](#).
- [53] Theodoros Papanikolaou, Vincent Vennin, and David Langlois, “Gravitational waves from a universe filled with primordial black holes,” JCAP **03**, 053 (2021), [arXiv:2010.11573 \[astro-ph.CO\]](#).
- [54] Guillem Domènech, Chunshan Lin, and Misao Sasaki, “Gravitational wave constraints on the primordial black hole dominated early universe,” JCAP **04**, 062 (2021), [Erratum: JCAP 11, E01 (2021)], [arXiv:2012.08151 \[gr-qc\]](#).
- [55] Gabriele Franciolini, *Primordial Black Holes: from Theory to Gravitational Wave Observations*, Ph.D. thesis, Geneva U., Dept. Theor. Phys. (2021), [arXiv:2110.06815 \[astro-ph.CO\]](#).
- [56] Junsong Cang, Yin-Zhe Ma, and Yu Gao, “Implications for Primordial Black Holes from Cosmological Constraints on Scalar-induced Gravitational Waves,” Astrophys. J. **949**, 64 (2023), [arXiv:2210.03476 \[astro-ph.CO\]](#).
- [57] Thomas C. Gehrman, Barnak Shams Es Haghi, Kuver Sinha, and Tao Xu, “Baryogenesis, primordial black holes and MHz–GHz gravitational waves,” JCAP **02**, 062 (2023), [arXiv:2211.08431 \[hep-ph\]](#).
- [58] Theodoros Papanikolaou, “Gravitational waves induced from primordial black hole fluctuations: the effect of an extended mass function,” JCAP **10**, 089 (2022), [arXiv:2207.11041 \[astro-ph.CO\]](#).



- [59] Taotao Qiu, Wenyi Wang, and Ruifeng Zheng, “Generation of primordial black holes from an inflation model with modified dispersion relation,” *Phys. Rev. D* **107**, 083018 (2023), [arXiv:2212.03403 \[astro-ph.CO\]](#).
- [60] Albert Escrivà, Florian Kuhnel, and Yuichiro Tada, “Primordial Black Holes,” (2022), [arXiv:2211.05767 \[astro-ph.CO\]](#).
- [61] Zhe Chang, Yu-Ting Kuang, Xukun Zhang, and Jing-Zhi Zhou, “Primordial black holes and third order scalar induced gravitational waves\*,” *Chin. Phys. C* **47**, 055104 (2023), [arXiv:2209.12404 \[astro-ph.CO\]](#).
- [62] Thomas C. Gehrman, Barmak Shams Es Haghi, Kuver Sinha, and Tao Xu, “The primordial black holes that disappeared: connections to dark matter and MHz-GHz gravitational Waves,” *JCAP* **10**, 001 (2023), [arXiv:2304.09194 \[hep-ph\]](#).
- [63] Giacomo Ferrante, Gabriele Franciolini, Antonio Iovino, Junior., and Alfredo Urbano, “Primordial black holes in the curvaton model: possible connections to pulsar timing arrays and dark matter,” *JCAP* **06**, 057 (2023), [arXiv:2305.13382 \[astro-ph.CO\]](#).
- [64] Bao-Min Gu, Fu-Wen Shu, and Ke Yang, “Inflation with shallow dip and primordial black holes,” (2023), [arXiv:2307.00510 \[astro-ph.CO\]](#).
- [65] Chen Yuan and Qing-Guo Huang, “Primordial Black Hole Interpretation in Subsolar Mass Gravitational Wave Candidate SSM200308,” (2024), [arXiv:2404.03328 \[astro-ph.CO\]](#).
- [66] Qing-Guo Huang, Chen Yuan, Zu-Cheng Chen, and Lang Liu, “GW230529\_181500: A Potential Primordial Binary Black Hole Merger in the Mass Gap,” (2024), [arXiv:2404.05691 \[gr-qc\]](#).
- [67] Chen Yuan and Qing-Guo Huang, “A topic review on probing primordial black hole dark matter with scalar induced gravitational waves,” (2021), [arXiv:2103.04739 \[astro-ph.GA\]](#).
- [68] Guillem Domènech, “Scalar Induced Gravitational Waves Review,” *Universe* **7**, 398 (2021), [arXiv:2109.01398 \[gr-qc\]](#).
- [69] B. P. Abbott *et al.* (LIGO Scientific, Virgo), “Observation of Gravitational Waves from a Binary Black Hole Merger,” *Phys. Rev. Lett.* **116**, 061102 (2016), [arXiv:1602.03837 \[gr-qc\]](#).
- [70] B. P. Abbott *et al.* (LIGO Scientific, Virgo), “Binary Black Hole Mergers in the first Advanced LIGO Observing Run,” *Phys. Rev. X* **6**, 041015 (2016), [Erratum: *Phys. Rev. X* **8**, 039903 (2018)], [arXiv:1606.04856 \[gr-qc\]](#).
- [71] B. P. Abbott *et al.* (LIGO Scientific, Virgo), “GWTC-1: A Gravitational-Wave Transient Catalog of Compact Binary Mergers Observed by LIGO and Virgo during the First and Second Observing Runs,” *Phys. Rev. X* **9**, 031040 (2019), [arXiv:1811.12907 \[astro-ph.HE\]](#).
- [72] R. Abbott *et al.* (LIGO Scientific, Virgo), “GWTC-2: Compact Binary Coalescences Observed by LIGO and Virgo During the First Half of the Third Observing Run,” *Phys. Rev. X* **11**, 021053 (2021), [arXiv:2010.14527 \[gr-qc\]](#).
- [73] R. Abbott *et al.* (LIGO Scientific, VIRGO), “GWTC-2.1: Deep extended catalog of compact binary coalescences observed by LIGO and Virgo during the first half of the third observing run,” *Phys. Rev. D* **109**, 022001 (2024), [arXiv:2108.01045 \[gr-qc\]](#).
- [74] R. Abbott *et al.* (KAGRA, VIRGO, LIGO Scientific), “GWTC-3: Compact Binary Coalescences Observed by LIGO and Virgo during the Second Part of the Third Observing Run,” *Phys. Rev. X* **13**, 041039 (2023), [arXiv:2111.03606 \[gr-qc\]](#).
- [75] Gabriella Agazie *et al.* (NANOGrav), “The NANOGrav 15 yr Data Set: Observations and Timing of 68 Millisecond Pulsars,” *Astrophys. J. Lett.* **951**, L9 (2023), [arXiv:2306.16217 \[astro-ph.HE\]](#).
- [76] Gabriella Agazie *et al.* (NANOGrav), “The NANOGrav 15 yr Data Set: Evidence for a Gravitational-wave Background,” *Astrophys. J. Lett.* **951**, L8 (2023), [arXiv:2306.16213 \[astro-ph.HE\]](#).
- [77] Adeela Afzal *et al.* (NANOGrav), “The NANOGrav 15 yr Data Set: Search for Signals from New Physics,” *Astrophys. J. Lett.* **951**, L11 (2023), [arXiv:2306.16219 \[astro-ph.HE\]](#).
- [78] Daniel J. Reardon *et al.*, “Search for an Isotropic Gravitational-wave Background with the Parkes Pulsar Timing Array,” *Astrophys. J. Lett.* **951**, L6 (2023), [arXiv:2306.16215 \[astro-ph.HE\]](#).
- [79] Andrew Zic *et al.*, “The Parkes Pulsar Timing Array third data release,” *Publ. Astron. Soc. Austral.* **40**, e049 (2023), [arXiv:2306.16230 \[astro-ph.HE\]](#).
- [80] J. Antoniadis *et al.* (EPTA), “The second data release from the European Pulsar Timing Array - I. The dataset and timing analysis,” *Astron. Astrophys.* **678**, A48 (2023), [arXiv:2306.16224 \[astro-ph.HE\]](#).
- [81] J. Antoniadis *et al.* (EPTA, InPTA), “The second data release from the European Pulsar Timing Array - III. Search for gravitational wave signals,” *Astron. Astrophys.* **678**, A50 (2023), [arXiv:2306.16214 \[astro-ph.HE\]](#).
- [82] J. Antoniadis *et al.* (EPTA), “The second data release from the European Pulsar Timing Array: V. Implications for massive black holes, dark matter and the early Universe,” (2023), [arXiv:2306.16227 \[astro-ph.CO\]](#).
- [83] Heng Xu *et al.*, “Searching for the Nano-Hertz Stochastic Gravitational Wave Background with the Chinese Pulsar Timing Array Data Release I,” *Res. Astron. Astrophys.* **23**, 075024 (2023), [arXiv:2306.16216 \[astro-ph.HE\]](#).
- [84] Yan-Chen Bi, Yu-Mei Wu, Zu-Cheng Chen, and Qing-Guo Huang, “Implications for the supermassive black hole binaries from the NANOGrav 15-year data set,” *Sci. China Phys. Mech. Astron.* **66**, 120402 (2023), [arXiv:2307.00722 \[astro-ph.CO\]](#).
- [85] Yu-Mei Wu, Zu-Cheng Chen, and Qing-Guo Huang, “Cosmological interpretation for the stochastic signal in pulsar timing arrays,” *Sci. China Phys. Mech. Astron.* **67**, 240412 (2024), [arXiv:2307.03141 \[astro-ph.CO\]](#).
- [86] Gabriele Franciolini, Antonio Iovino, Junior., Ville Vaskonen, and Hardi Veermae, “Recent Gravitational Wave Observation by Pulsar Timing Arrays and Primordial Black Holes: The Importance of Non-Gaussianities,” *Phys. Rev. Lett.* **131**, 201401 (2023), [arXiv:2306.17149 \[astro-ph.CO\]](#).
- [87] Keisuke Inomata, Kazunori Kohri, and Takahiro Terada, “Detected stochastic gravitational waves and subsolar-mass primordial black holes,” *Phys. Rev. D* **109**, 063506 (2024), [arXiv:2306.17834 \[astro-ph.CO\]](#).
- [88] Lang Liu, Zu-Cheng Chen, and Qing-Guo Huang, “Implications for the non-Gaussianity of curvature perturbation from pulsar timing arrays,” *Phys. Rev. D* **109**, L061301 (2024), [arXiv:2307.01102 \[astro-ph.CO\]](#).
- [89] Zhu Yi, Qing Gao, Yungui Gong, Yue Wang, and Fengge Zhang, “Scalar induced gravitational waves in light of Pulsar

- Timing Array data,” *Sci. China Phys. Mech. Astron.* **66**, 120404 (2023), arXiv:2307.02467 [gr-qc].
- [90] Zhi-Qiang You, Zhu Yi, and You Wu, “Constraints on primordial curvature power spectrum with pulsar timing arrays,” *JCAP* **11**, 065 (2023), arXiv:2307.04419 [gr-qc].
- [91] Jia-Heng Jin, Zu-Cheng Chen, Zhu Yi, Zhi-Qiang You, Lang Liu, and You Wu, “Confronting sound speed resonance with pulsar timing arrays,” *JCAP* **09**, 016 (2023), arXiv:2307.08687 [astro-ph.CO].
- [92] Shyam Balaji, Guillem Domènech, and Gabriele Franciolini, “Scalar-induced gravitational wave interpretation of PTA data: the role of scalar fluctuation propagation speed,” *JCAP* **10**, 041 (2023), arXiv:2307.08552 [gr-qc].
- [93] Spyros Basilakos, Dimitri V. Nanopoulos, Theodoros Papanikolaou, Emmanuel N. Saridakis, and Charalampos Tzerefos, “Gravitational wave signatures of no-scale supergravity in NANOGrav and beyond,” *Phys. Lett. B* **850**, 138507 (2024), arXiv:2307.08601 [hep-th].
- [94] Lang Liu, Zu-Cheng Chen, and Qing-Guo Huang, “Probing the equation of state of the early Universe with pulsar timing arrays,” *JCAP* **11**, 071 (2023), arXiv:2307.14911 [astro-ph.CO].
- [95] Spyros Basilakos, Dimitri V. Nanopoulos, Theodoros Papanikolaou, Emmanuel N. Saridakis, and Charalampos Tzerefos, “Induced gravitational waves from flipped SU(5) superstring theory at nHz,” *Phys. Lett. B* **849**, 138446 (2024), arXiv:2309.15820 [astro-ph.CO].
- [96] Pau Amaro-Seoane *et al.* (LISA), “Laser Interferometer Space Antenna,” (2017), arXiv:1702.00786 [astro-ph.IM].
- [97] Wen-Hong Ruan, Zong-Kuan Guo, Rong-Gen Cai, and Yuan-Zhong Zhang, “Taiji program: Gravitational-wave sources,” *Int. J. Mod. Phys. A* **35**, 2050075 (2020), arXiv:1807.09495 [gr-qc].
- [98] Jun Luo *et al.* (TianQin), “TianQin: a space-borne gravitational wave detector,” *Class. Quant. Grav.* **33**, 035010 (2016), arXiv:1512.02076 [astro-ph.IM].
- [99] Seiji Kawamura *et al.*, “Current status of space gravitational wave antenna DECIGO and B-DECIGO,” *PTEP* **2021**, 05A105 (2021), arXiv:2006.13545 [gr-qc].
- [100] N. Bartolo, V. De Luca, G. Franciolini, A. Lewis, M. Peloso, and A. Riotto, “Primordial Black Hole Dark Matter: LISA Serendipity,” *Phys. Rev. Lett.* **122**, 211301 (2019), arXiv:1810.12218 [astro-ph.CO].
- [101] N. Bartolo, V. De Luca, G. Franciolini, M. Peloso, D. Racco, and A. Riotto, “Testing primordial black holes as dark matter with LISA,” *Phys. Rev. D* **99**, 103521 (2019), arXiv:1810.12224 [astro-ph.CO].
- [102] Bernard Carr, Kazunori Kohri, Yuuiti Sendouda, and Jun’ichi Yokoyama, “Constraints on primordial black holes,” *Rept. Prog. Phys.* **84**, 116902 (2021), arXiv:2002.12778 [astro-ph.CO].
- [103] Shi Pi and Misao Sasaki, “Gravitational Waves Induced by Scalar Perturbations with a Lognormal Peak,” *JCAP* **09**, 037 (2020), arXiv:2005.12306 [gr-qc].
- [104] Guillermo Ballesteros and Marco Taoso, “Primordial black hole dark matter from single field inflation,” *Phys. Rev. D* **97**, 023501 (2018), arXiv:1709.05565 [hep-ph].
- [105] Pedro Carrilho, Karim A. Malik, and David J. Mulryne, “Dissecting the growth of the power spectrum for primordial black holes,” *Phys. Rev. D* **100**, 103529 (2019), arXiv:1907.05237 [astro-ph.CO].
- [106] Keitaro Tomikawa and Tsutomu Kobayashi, “Gauge dependence of gravitational waves generated at second order from scalar perturbations,” *Phys. Rev. D* **101**, 083529 (2020), arXiv:1910.01880 [gr-qc].
- [107] V. De Luca, G. Franciolini, A. Kehagias, and A. Riotto, “On the Gauge Invariance of Cosmological Gravitational Waves,” *JCAP* **03**, 014 (2020), arXiv:1911.09689 [gr-qc].
- [108] Keisuke Inomata and Takahiro Terada, “Gauge Independence of Induced Gravitational Waves,” *Phys. Rev. D* **101**, 023523 (2020), arXiv:1912.00785 [gr-qc].
- [109] Chen Yuan, Zu-Cheng Chen, and Qing-Guo Huang, “Scalar induced gravitational waves in different gauges,” *Phys. Rev. D* **101**, 063018 (2020), arXiv:1912.00885 [astro-ph.CO].
- [110] Massimo Giovannini, “Spurious gauge-invariance of higher-order contributions to the spectral energy density of the relic gravitons,” *Int. J. Mod. Phys. A* **35**, 2050165 (2020), arXiv:2005.04962 [hep-th].
- [111] Yizhou Lu, Arshad Ali, Yungui Gong, Jiong Lin, and Fengge Zhang, “Gauge transformation of scalar induced gravitational waves,” *Phys. Rev. D* **102**, 083503 (2020), arXiv:2006.03450 [gr-qc].
- [112] Jun-Peng Li, Sai Wang, Zhi-Chao Zhao, and Kazunori Kohri, “Complete analysis of the background and anisotropies of scalar-induced gravitational waves: primordial non-Gaussianity  $f_{NL}$  and  $g_{NL}$  considered,” *JCAP* **06**, 039 (2024), arXiv:2309.07792 [astro-ph.CO].
- [113] Gabriele Perna, Chiara Testini, Angelo Ricciardone, and Sabino Matarrese, “Fully non-Gaussian Scalar-Induced Gravitational Waves,” *JCAP* **05**, 086 (2024), arXiv:2403.06962 [astro-ph.CO].
- [114] Katsuya T. Abe, Yuichiro Tada, and Ikumi Ueda, “Induced gravitational waves as a cosmological probe of the sound speed during the QCD phase transition,” *JCAP* **06**, 048 (2021), arXiv:2010.06193 [astro-ph.CO].